Thermochronologic evaluation of postcollision extension in the Anatolide orogen, western Turkey

Stuart N. Thomson[1] and Uwe Ring[2]

Received 12 April 2005; revised 13 November 2005; accepted 10 February 2006; published 9 May 2006.

[1] To better understand the driving mechanisms behind the transition from collision to extension in a convergent orogen, data from multiple low-temperature thermochronometers were obtained from the Simav detachment fault (SDF), the earliest developed major extensional structure recognized in the western Anatolide orogen of western Turkey. Twenty-two zircon fission track (FT), 26 apatite FT, 12 apatite (U-Th)/He ages, and 26 apatite FT track length analyses are presented. The data establish that the SDF was a major extensional fault active between ~25 and ~19 Ma. The coincidence in timing of magmatism with cessation of SDF activity implies the detachment became locked owing to doming induced by magma emplacement. Zircon FT ages away from the influence of Miocene magmatism record rapid footwall cooling between ~25 and ~21 Ma at a slip rate of up to ~15 km/Myr and demonstrate that active ductile deformation along the SDF migrated northward with time. Apatite FT ages from the footwall of the SDF are spatially invariant over >100 km and consistently ~2–3 Myr younger than the zircon fission track ages from the same samples. These data are consistent with a regional, but relatively rapid erosion-linked cooling phase that removed ~2–3 km of overburden following cessation of SDF activity but before deposition of sedimentary rocks on the detachment surface at 16.4 Ma. Postcollision extension of the Anatolide orogen with development of the SDF can be best explained as the result of postcollision magmatism and thermal weakening of the crust inducing the extensional reactivation of an earlier major out-of-sequence thrust. **Citation:** Thomson, S. N., and U. Ring (2006), Thermochronologic evaluation of postcollision extension in the Anatolide orogen, western Turkey, *Tectonics*, *25*, TC3005, doi:10.1029/2005TC001833.

1. Introduction

[2] Crustal extension during or following convergent orogenesis is a phenomenon now recognized in most modern and ancient orogens worldwide [e.g., *Dewey*, 1988]. However, the character and magnitude of extension, the geodynamic forces driving extension, and the relative timing of extension with respect to crustal shortening can vary significantly between different orogens and even within the same orogen. In a number of active orogens extensional faulting has been shown to be synchronous with convergent orogenesis: e.g., the Apennines [*Carmignani and Kligfield*, 1990], Aegean Sea [*Lister et al.*, 1984], Hellenic Arc [*Fassoulas et al.*, 1994], and the Himalaya [*Burchfiel and Royden*, 1985]. Geodynamic models to explain synorogenic extension are varied, and include back-arc extension related to slab pull or mantle corner flow [e.g., *Mantovani et al.*, 2001], buoyant escape following crust-lithosphere detachment [*Chemenda et al.*, 1995; *Thomson et al.*, 1999], or extensional thinning of an over thickened critical orogenic wedge [e.g., *Platt*, 1986]. In many other modern and ancient orogens, extension is a late or postcrustal thickening occurrence, often leading to extreme thinning with the development of metamorphic core complexes, and even oceanic crust. Examples include the Basin and Range province [*Sonder and Jones*, 1999], Alboran Sea [*Platt and Vissers*, 1989], and the more ancient Variscan [*Malavieille*, 1993] and Scandinavian Caledonide [*Fossen*, 1999] orogens. Most models of late and postorogenic extension invoke either extensional collapse driven by gravity and/or thermal instability (see reviews by *Liu* [2001] and *Rey et al.* [2001]), and/or removal of a lithospheric root, by delamination, convection, or slab break off [e.g., *England and Houseman*, 1989; *Platt et al.*, 2003].

[3] To determine which geodynamic model or combination of models best describes the driving forces behind the presence of crustal extension within a particular convergent orogen thus depends critically on being able to accurately and precisely determine the timing, rates, magnitude, and style of extension and its relation in time and space to associated magmatism, sedimentation, and convergent tectonics. In this study we attempt such an evaluation by integrating new results from multiple low-temperature thermochronometers with preexisting structural, magmatic and sedimentologic information from the Anatolide orogen of western Turkey (Figure 1). This is now recognized as a region that has undergone extreme late Cenozoic horizontal extension and vertical thinning following a prolonged period of Late Cretaceous to Eocene crustal shortening concluding with the late Eocene to early Oligocene collision of the exotic Anatolide microcontinent at the active Eurasian continental margin. The crustal dynamic processes that led to the transition from collision to extension remain equivocal and contentious. Numerous alternate models have

[1]Department of Geology and Geophysics, Yale University, New Haven, Connecticut, USA.
[2]Department of Geological Sciences, University of Canterbury, Christchurch, New Zealand.

0278-7407/06/2005TC001833

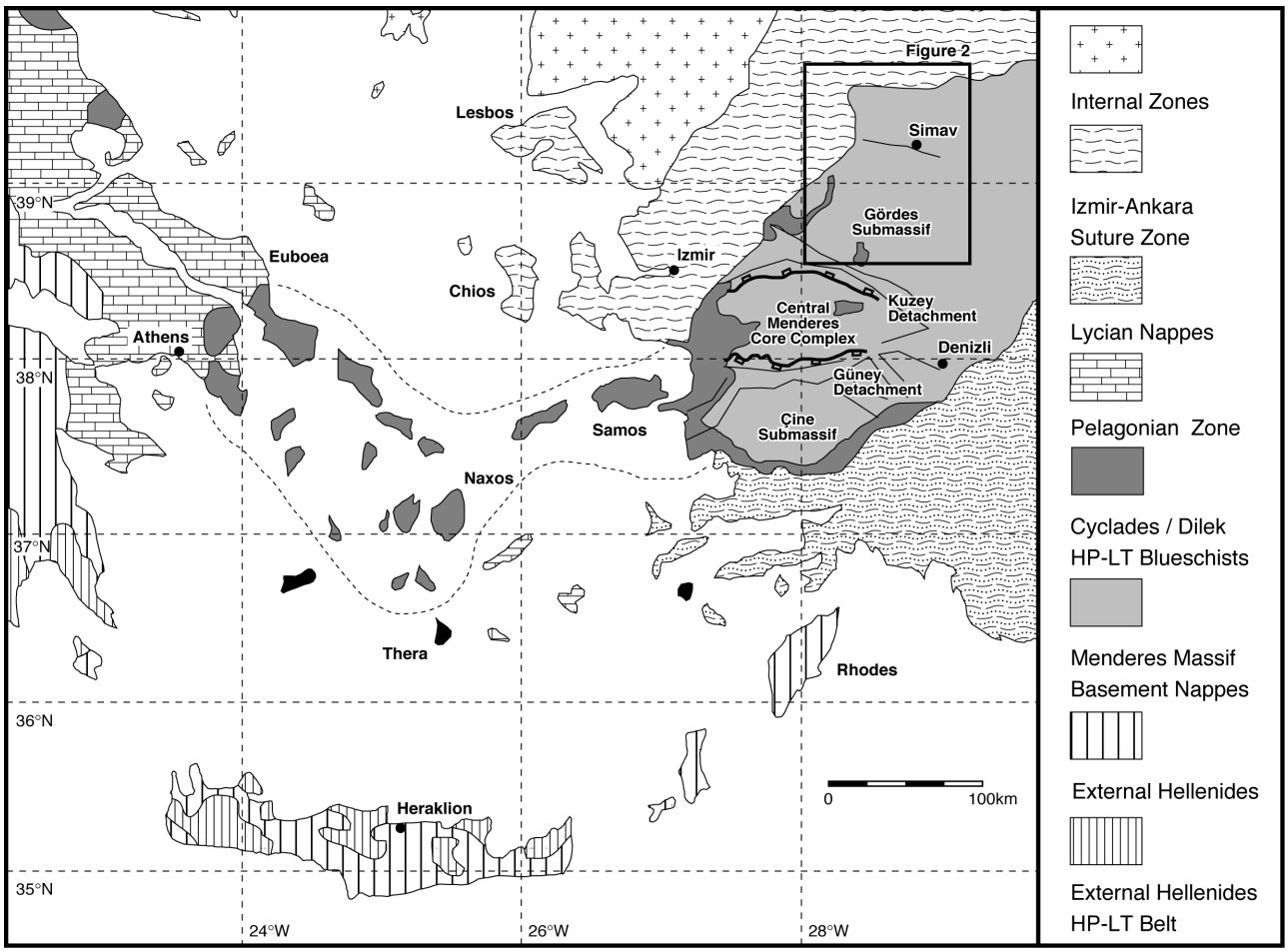

Figure 1. Generalized tectonic map of the Aegean and western Turkey showing the major tectonic subdivisions of the Hellenide and western Anatolide orogens.

been invoked (see reviews by *Seyitoğlu and Scott* [1996], *Aldanmaz et al.* [2000], and *Bozkurt* [2003]) including (1) gravitational collapse of previously thickened crust; (2) lithospheric delamination or slab detachment; (3) back-arc extension caused by retreat of the Hellenic subduction zone; (4) extension related to the westward ''tectonic escape'' of the Anatolian microplate; or (5) any combination of the above mechanisms. The timing, magnitude, and style of younger Miocene-Recent extension in western Turkey is now generally well recognized and accepted. It includes the late Miocene to Recent formation of the central Menderes metamorphic core complex, bound to both the north and south by major extensional detachment faults [e.g., *Gessner et al.*, 2001a], and the development of numerous Neogene-Recent E-W trending grabens [*Şengör*, 1987; *Seyitoğlu and Scott*, 1992, 1996; *Koçyiğit et al.*, 1999; *Seyitoğlu et al.*, 2000; *Bozkurt*, 2003; *Purvis and Robertson*, 2004a, 2004b]. However, the time of onset, and nature of the earliest post-collision extension in western Anatolia remains contentious [*Seyitoğlu et al.*, 1992, 2004; *Seyitoğlu and Scott*, 1996; *Yilmaz et al.*, 2000; *Bozkurt*, 2003; *Ring et al.*, 2003a; *Purvis and Robertson*, 2004a, 2004b; *Catlos and Çemen*, 2005].

[4] To help resolve these arguments, we have applied fission track and (U-Th)/He thermochronometry to an extensive suite of samples collected from both the footwall and hanging wall rocks of the Simav detachment fault (SDF) at the northern margin of the Anatolide orogen. The SDF is the only tectonic contact in the Anatolide orogen that is universally recognized as recording early postcollision extension in late Oligocene to early Miocene times [*Işik and Tekeli*, 2001; *Işik et al.*, 2003; 2004; *Ring et al.*, 2003a; *Seyitoğlu et al.*, 2004; *Ring and Collins*, 2005].

2. Anatolide Orogen of Western Turkey

[5] The Anatolide orogen comprises a Late Cretaceous to Eocene largely south vergent accretionary belt with local high-pressure metamorphism formed during crustal shortening related to northward directed subduction of Neotethys beneath the active Eurasian margin [*Ring et al.*, 1999, 2001a; *Okay*, 2001; *Gessner et al.*, 2001b]. These rocks were later disrupted by the late Eocene to early Oligocene collision of the exotic Anatolide microcontinent with Eurasia [*Gessner et al.*, 2001c; *Ring and Layer*, 2003], which

now forms the distinctive Late Precambrian/Cambrian basement in the region.

[6] The former Eurasian margin in western Turkey forms the "Internal Zone" (Figure 1), an amalgamation of Triassic greenschist-, blueschist- and eclogite-facies metamorphic rocks [*Bozkurt and Oberhänsli*, 2001]. The Late Cretaceous to Eocene accretionary complex, referred to as the Anatolide orogen, comprises three main tectonometamorphic zones. From top to bottom these are: (1) İzmir-Ankara suture zone/Lycian nappes; (2) the Cyclades blueschist unit; and (3) the Menderes nappes.

[7] The İzmir-Ankara suture zone represents a suite of high-pressure low-temperature (HP-LT) and greenschist facies rocks of the former Eurasian continental margin accreted and metamorphosed from Late Cretaceous to Eocene times at the former subduction zone of Neotethys beneath Eurasia [*Şengör and Yilmaz*, 1981; *Sherlock et al.*, 1999; *Bozkurt and Oberhänsli*, 2001] overlain by the Late Cretaceous-Paleocene ophiolitic Bornova flysch [*Okay and Siyako*, 1993].

[8] The Lycian nappes are a series of thrust sheets that were emplaced episodically from Late Cretaceous to Miocene times southeastward over rocks of the Cyclades blueschist unit and Menderes nappes. They comprise both ophiolitic mélange and rocks of the former southern passive margin of Neotethys and are restricted to the south and west side of the Menderes Massif (Figure 1) in a similar tectonic position to the İzmir-Ankara zone [*Collins and Robertson*, 1997, 1999; *Ring et al.*, 1999; *Ring and Layer*, 2003].

[9] The İzmir Ankara suture zone and the Lycian nappes lie tectonically above the high-pressure-low-temperature Cyclades blueschist unit [*Ring et al.*, 1999]. These rocks record a younger Paleocene-Eocene (~55 Ma) deformation and metamorphic history [*Sherlock et al.*, 1999; *Tomaschek et al.*, 2003; *Ring and Layer*, 2003]. In the middle to late Eocene, during collision of the Anatolide microcontinent, the Cyclades blueschist unit rocks were emplaced onto the Menderes nappes of western Turkey by the out-of-sequence Cyclades-Menderes thrust [*Gessner et al.*, 2001b].

[10] The Menderes nappes form the lowest exposed part of the Anatolide orogen in western Turkey. Detailed geologic, structural, and geochronologic examination of the Menderes nappes [e.g., *Ring et al.*, 1999; *Gessner et al.*, 2001a, 2001b; *Okay*, 2001] demonstrates that they represent the accreted remnants of an exotic continental block (the Anatolia microcontinent) of Pan-African affinity, with localized deformation related to Alpine nappe emplacement. Four main Menderes nappes can be distinguished that were juxtaposed in the Eocene during greenschist facies out-of-sequence thrusting [*Ring et al.*, 1999]. From top to bottom these are labeled the Selimiye nappe, the Çine nappe, the Bozdağ nappe, and the Bayındır nappe.

3. Postorogenic Extension and the Simav Detachment

[11] Following the cessation of Anatolide collision sometime in the early Oligocene, western Turkey underwent a transition to a dominantly N-S extensional tectonic regime. Postorogenic extension is most obviously manifest by the presence of two phases of late Cenozoic-Recent graben formation with associated coeval deposition of thick volcanosedimentary successions [*Yilmaz et al.*, 2000; *Bozkurt*, 2003; *Purvis and Robertson*, 2004a, 2004b]. Older approximately N-S trending basins, including the Gördes and Selendi basins of the Gördes submassif (Figure 2a), record early to middle Miocene extension. These are cut by a set of younger approximately E-W trending Pliocene-Recent grabens, including the prominent Gediz (or Alaşehir) and Büyük Menderes grabens [*Cohen et al.*, 1995].

[12] As well as graben formation, the discovery of major late Cenozoic extensional detachments and metamorphic core complexes in the Aegean [e.g., *Lister et al.*, 1984] led to the recognition that many of the tectonic contacts in neighboring western Turkey were also major low-angle extensional detachment faults [*Hetzel et al.*, 1995; *Gessner et al.*, 2001a; *Seyitoğlu et al.*, 2000, 2002; *Işik and Tekeli*, 2001; *Işik et al.*, 2003; *Ring et al.*, 2003a]. Thermochronology, structural and stratigraphic field relationships, and synkinematic magmatism reveal that this extensional detachment faulting occurred in two phases [*Gessner et al.*, 2001a; *Ring et al.*, 2003a; *Catlos and Çemen*, 2005]: one in the latest Oligocene to early Miocene that affected the upper structural levels of the Anatolide orogen, and a later Pliocene to Recent phase resulting in the development of a large bivergent metamorphic core complex in the central Anatolide orogen. Older synorogenic extensional shear zones may also exist within the Anatolide orogen. For example, *Gessner et al.* [2001c] discuss the possibility that Eocene exhumation of high-pressure rocks of the Cyclades blueschist unit may have been aided by an extensional shear zone, coeval with the emplacement of these rocks on the Menderes nappes along the out-of-sequence Cyclades-Menderes thrust. However, these faults did not result in core complex formation and are unrelated to postorogenic unroofing of the Anatolide orogen [*Ring and Collins*, 2005].

[13] The younger Pliocene to Recent detachment faulting in the central Anatolide orogen is dominated by two E-W striking, approximately symmetric detachment systems; the top-to-north Kuzey (or Alaşehir) detachment, and the top-to-the south Güney (or Büyük Menderes) detachment, which define the northern and southern boundary, respectively, of the Central Menderes metamorphic core complex [*Gessner et al.*, 2001a] (Figure 2). Cooling ages from the footwall rocks of the Kuzey detachment establish that unroofing along this fault was active at ~5 Ma [*Gessner et al.*, 2001a; *Seyitoğlu et al.*, 2000, 2002] and perhaps as early as the Miocene [*Catlos and Çemen*, 2005].

[14] The nature of older late Oligocene to early Miocene postorogenic unroofing in the Anatolide orogen is more disputed (cf. *Ring et al.* [2003a] versus *Seyitoğlu et al.* [2004]). The most widely accepted example of an early postcollision detachment fault is the Simav detachment fault (SDF) at the northern margin of the Anatolide orogen, first described by *Işik and Tekeli* [2001] (Figure 2a). The hanging wall of the SDF consists of highly disrupted schist, marble, and ophiolitic flysch of the Cyclades blueschist unit and the İzmir-Ankara suture zone [*Işik and Tekeli*, 2001;

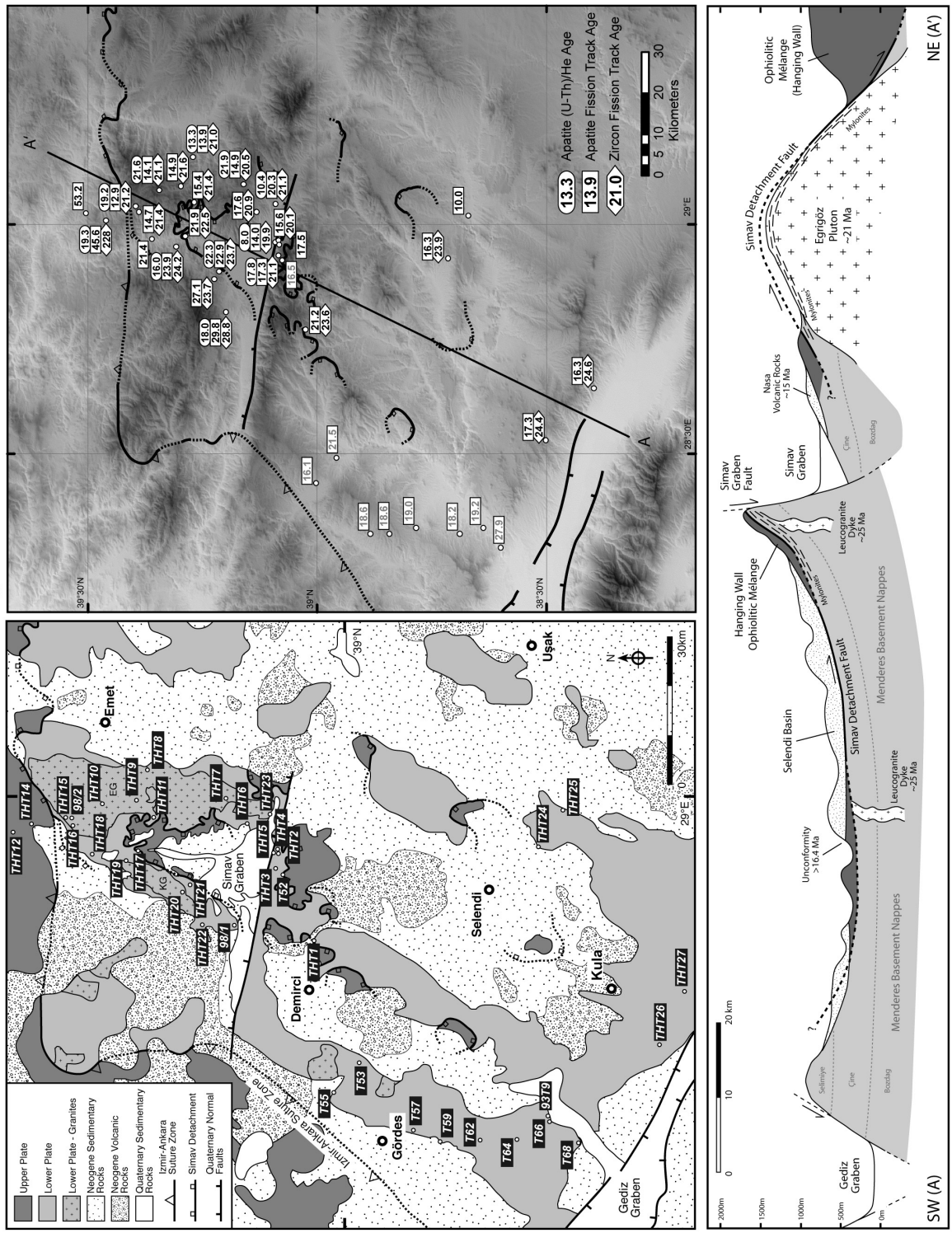
a
Upper Plate
Lower Plate
Lower Plate - Granites
Neogene Sedimentary Rocks
Neogene Volcanic Rocks
Quaternary Sedimentary Rocks
Izmir-Ankara Suture Zone
Simav Detachment
Quaternary Normal Faults
İzmir-Ankara Suture Zone
Emet
Simav Graben
Demirci
Selendi
Kula
Uşak
Gördes
Gediz Graben
KG
EG
39°N
29°E
30km
b
A
A'
38°30'N
39°N
29°30'E
29°E
Apatite (U-Th)/He Age
Apatite Fission Track Age
Zircon Fission Track Age
Kilometers
c
SW (A)
NE (A')
Hanging Wall Ophiolitic Mélange
Selendi Basin
Simav Detachment Fault
Unconformity >16.4 Ma
Leucogranite Dyke ~25 Ma
Menderes Basement Nappes
Simav Graben Fault
Simav Graben
Nasa Volcanic Rocks ~15 Ma
Egrigöz Pluton ~21 Ma
Mylonites
Ophiolitic Mélange (Hanging Wall)
Gediz Graben
Selimiye
Çine
Bozdağ
20 km
2000m
1500m
1000m
500m
0m

Figure 2

Ring et al., 2003a]. The footwall comprises Precambrian gneisses of the Menderes Çine and Bozdağ nappes, and is locally intruded by two synkinematic early Miocene (~21 Ma) granites: the Eğrigöz and Koyunoba granites (EG and KG in Figure 2a) [*Işik et al.*, 2004; *Ring and Collins*, 2005]. Progressive deformation from ductile to brittle conditions is preserved; the mylonites being cut by later brittle microfaults, and locally brecciated to form cataclasite, ultracataclasite, and occasional pseudotachylite [*Ring and Collins*, 2005]. Very rapid postemplacement cooling of the granites is implied by their near concordant ~21–20 Ma U-Th-Pb SIMS zircon intrusion ages and independent $^{40}Ar/^{39}Ar$ mica cooling ages [*Işik et al.*, 2004; *Ring and Collins*, 2005]. Reconnaissance apatite fission track (FT) cooling ages [*Gessner et al.*, 2001a; *Ring et al.*, 2003a] from the Gördes submassif are similar or slightly younger than the age of granite intrusion at 21–16 Ma. *Ring et al.* [2003a] infer a slight northward younging trend of these apatite FT ages in the direction of tectonic transport on the SDF, which they interpret as cooling related to tectonic unroofing of the hanging wall at a slip rate of ~10 km/Myr. The total extensional displacement along the SDF cannot be reliably determined from offset geologic markers, as rocks either side of the detachment represent units formerly juxtaposed by the earlier out-of-sequence Cyclades-Menderes thrust. The timing of cessation of movement along the SDF is constrained by 15.8–15.3 Ma volcano-sedimentary rocks deposited on the Simav detachment surface (*Ercan et al.* [1997], cited by *Işik et al.* [2004]). *Purvis and Robertson* [2004a] argue that these sedimentary deposits (which they date to between 21.7 ± 0.1 Ma and 16.4 ± 0.1 Ma) represent supradetachment basins deposited in depressions or corrugations of the former detachment surface. However, the top-to-the-NE structures they use as evidence for a detachment surface are not themselves dated. In fact these structures are more analogous to the much older Pan-African top-to-the-NE ductile deformation observed throughout the Çine nappe (compare Figure 4c of *Purvis and Robertson* [2004a, 2004b] and Figure 4b of *Gessner et al.* [2001b]).

[15] Oligo-Miocene postcollision detachment faulting has also been proposed for the top-to-the-SSW Selimiye shear zone at the southern margin of the Anatolide orogen (the Çine submassif, Figure 1) [e.g., *Bozkurt and Park*, 1994; *Bozkurt and Satir*, 2000], although others [e.g., *Ring et al.*, 1999; 2003a; *Régnier et al.*, 2003] argue that the Selimiye shear zone was in fact a thrust that was later rotated to give an impression of extensional fault geometry. *Seyitoğlu et al.* [2004] present an alternative working hypothesis for Oligo-Miocene exhumation of the southern Çine submassif. They propose an originally north dipping top-to-the-NNE breakaway fault linked to the SDF in the north as part of an orogen-scale detachment fault that caused initial postcollision exhumation of the Menderes massif as part of a large metamorphic core complex active in late Oligocene to Miocene times.

4. Low-temperature Thermochronology

4.1. Fission Track Analysis

[16] Apatite and zircon crystals were separated, mounted, polished, and etched according to the techniques outlined by *Hurford et al.* [1991]. The samples were analyzed applying the external detector method and irradiated at the Oregon State University Triga Reactor, Corvallis. The neutron fluence was monitored using Corning uranium-dosed glasses CN5 for apatite and CN2 for zircon. Spontaneous and induced FT densities were counted using a Zeiss Axioplan microscope at 1250 times magnification. Apatite FT lengths were measured using an attached drawing tube and digitizing tablet calibrated against a stage micrometer. Central ages [*Galbraith and Laslett*, 1993], quoted with 2σ errors, were calculated using the IUGS recommended Zeta calibration approach of *Hurford and Green* [1983]. CN5 apatite and CN2 zircon zeta calibration factors of 358.8 ± 12.7 and 130.7 ± 2.8 Ma, respectively, were obtained by repeated calibration against a number of internationally agreed age standards according to the recommendations of *Hurford* [1990]. Fission tracks in both apatite and zircon shorten or anneal with increased temperature and duration of heating. For apatite of typical Durango composition (0.4 wt% Cl) experimental and borehole data [e.g., *Green et al.*, 1989; *Ketcham et al.*, 1999] show that over geologic time tracks begin to anneal at a sufficient rate to be measurable above ~60°C, with complete annealing and total resetting of the apatite fission track age occurring at between 100°C and 120°C. This range of temperatures is usually labeled the apatite fission track partial annealing zone (APAZ). For samples that have undergone moderate to fast cooling, a value of 100 ± 20°C can reasonably be assumed for the closure temperature of fission tracks in apatite. In zircon, tracks are stable to higher temperatures. For pristine zircon, annealing over geologic time begins at about 250 ± 20°C, with total resetting occurring above about 310 ± 20°C [*Tagami et al.*, 1998], although these temperatures are lower in zircons with high accumulated radiation damage [*Brandon et al.*, 1998; *Rahn et al.*, 2004]. This translates into a closure temperature for fission tracks

Figure 2. (a) Simplified geologic map of the northern Menderes massif (Gördes submassif) around the area of Simav. Numbers refer to samples analyzed and discussed in this study (THT from this study, T52-T68 and 93T9 fission track and $^{40}Ar/^{39}Ar$ samples from *Gessner et al.* [2001a] and *Ring et al.* [2003a], and 98/1 and 98/2 from *Işik et al.* [2004]). Outcrop of Simav detachment based on the works by *Işik and Tekeli* [2001] and *Işik et al.* [2003]. (b) Map showing fission track and (U-Th)/He ages obtained in this study (black) and presented by *Gessner et al.* [2001c] and *Ring et al.* [2003a] (grey). Shaded relief map is based on SRTM 90 m digital elevation data. (c) NNE-SSW schematic geologic cross section showing Simav detachment fault (SDF). Note postkinematic doming of the fault surface and its offset by the younger Simav Graben fault.

in zircon at moderate to fast cooling rates of 280 ± 30°C [*Stöckhert et al.*, 1999].

4.2. (U-Th)/He Dating

[17] Dated crystals were handpicked from the fission track separates, and inspected under a high-powered binocular microscope with cross polarization to eliminate grains with inclusions. Suitable grains were then measured in two orientations for later alpha ejection correction, and loaded either as single or multiple grains into 1 mm Pt tubes. Degassing of He was achieved by heating with a Nd-YAG laser in a high-vacuum laser cell connected to the He extraction and measurement line. Concentration of ^{4}He was determined by spiking with a known volume of ^{3}He and analyzing the isotope ratio in a quadrupole mass spectrometer according to the procedure outlined by *Reiners et al.* [2003]. For U and Th analysis, degassed apatite grains were dissolved in situ from Pt tubes in HNO_3 and spiked with a calibrated ^{229}Th and ^{233}U solution. U and Th concentrations were determined by inductively coupled plasma mass spectrometry. Alpha ejection was corrected using the formula of *Farley* [2002]. On the basis of the long-term reproducibility of Durango apatite standard analyses at Yale University, an analytical uncertainty of 6% (2σ) was applied to the apatite (U-Th)/He age determinations. Radiogenic He accumulated in apatite is lost by diffusion at even lower temperatures than the annealing of fission tracks in the same mineral. Extrapolation of laboratory He diffusion experiments in apatite to geologic time [*Farley*, 2000], supported by evidence from borehole data [*House et al.*, 1999], show that He begins to be measurably lost above about 45°C, and entirely lost above about 85°C for a typical grain with radius of 60 ± 20 μm [*Wolf et al.*, 1998]. This range of temperatures, commonly labeled the helium partial retention zone (HePRZ), is analogous to the APAZ. For a similar sized grain cooling at a rate of ~10°C/Myr, the closure temperature for He in apatite is ~70°C [*Farley*, 2000].

4.3. Sampling Strategy

[18] Samples for this study were collected to supplement and expand the reconnaissance thermochronologic results from the northern part of the Menderes Massif published by *Gessner et al.* [2001c] and *Ring et al.* [2003a]. To best estimate variables including the timing, onset, and duration of extension, the rates and amounts of fault slip, initial fault geometry, and the extent of synkinematic plutonism, we collected a further 27 samples from the footwall and hanging wall of the SDF as mapped by *Işik and Tekeli* [2001]. From the footwall we collected 14 samples from quartzites, schists, leucogranite dikes, and mylonites of the Çine nappe, 7 samples from the Eğrigöz granite, and 3 samples from the Koyunoba granite. In addition, 3 samples were taken from ophiolitic flysch of the İzmir-Ankara suture zone in the hanging wall of the detachment, north of its northernmost surface expression (Figures 2a and 2b). Unfortunately, the ophiolitic nature of the hanging wall klippen of the SDF (or Menderes-Cyclades thrust) south of Simav town (Figure 2) precluded the collection of apatite and zircon for thermochronologic analysis. From several samples collected, none yielded any zircon or apatite. In an attempt to better estimate fault slip rates we collected samples, where possible, at regular intervals parallel to the top-to-the-NNE hanging wall transport direction [e.g., *Foster et al.*, 1993; *Foster and John*, 1999]. Several samples were also collected from a high-relief (~600 m) transect just south of the Simav town (i.e., approximately perpendicular to the detachment surface) in an attempt to investigate the contribution of postdetachment erosion to footwall exhumation.

4.4. Summary of Results

[19] From 27 new samples collected from the footwall and hanging wall of the SDF, we present 22 zircon fission track (ZFT) ages, 26 apatite fission track (AFT) ages, and 26 AFT mean track length analyses (Table 1), as well as 12 new apatite (U-Th)/He (AHe) ages (Table 2). The geographic distribution of new ages is shown in Figure 2c, together with previously published fission track ages from *Gessner et al.* [2001c] and *Ring et al.* [2003a]. The 21 ZFT ages from the footwall of the Simav detachment, including the Eğrigöz and Koyunoba granites, range between 19.9 ± 1.7 and 28.8 ± 2.0 Ma (errors quoted at ±2σ). All these ages have low age dispersion (<6%) and pass the χ^2 test at the 5% level, indicating that the single grain ages used to calculate the central age were derived from one age population [*Galbraith and Laslett*, 1993]. A single ZFT age from the hanging wall of the SDF gives an age of 228 ± 23 Ma, significantly older than the ZFT ages from the footwall rocks. The 24 AFT ages from the footwall of the SDF show more variation, ranging from 10.0 ± 2.4 to 29.8 ± 4.5 Ma. The AFT ages all show low age dispersion (<5%). Good quality apatite track length analyses (with large numbers of measured tracks) were obtained from most samples. The mean AFT track lengths are all, with one exception, above 14 μm, with low standard deviations (<1.6 μm), typical for samples that cooled quickly through the AFT partial annealing zone (APAZ) from ~110°C to below ~60°C at about the time represented by the AFT age [e.g., *Green et al.*, 1989]. The ophiolitic flysch from the hanging wall of the SDF yielded two AFT ages of 45.6 ± 6.1 Ma and 53.2 ± 20.9 Ma, both significantly older than the AFT ages from the footwall rocks. The higher precision sample (THT14) has a unimodal, negatively skewed confined AFT track length distribution with a mean length of 13.3 μm and standard deviation of 2.07 μm. Such a distribution is typical for a sample that cooled slowly, but monotonically through the APAZ [*Gallagher et al.*, 1998] at about the time represented by the AFT age.

[20] To provide an independent constraint for the results of AFT analysis and to provide more precise lower temperature thermochronologic constraints, 16 AHe age analyses were performed on selected samples; 11 from the footwall of the SDF, 1 from the hanging wall of the SDF, plus 4 replicate analyses on samples where the initial AHe age was apparently anomalously old (i.e., significantly older than the AFT age). Anomalously old AHe ages from samples THT1A, THT7A, THT8A, and THT15B (Table 2) are omitted from data analysis and interpretation, as in these samples we

Table 1. Apatite and Zircon Fission Track Data[a]

Sample	Elevation, m	Location (WGS84) (Rock Type)	Rock Type (Unit/Nappe)	Mineral	Number of Crystals	Track Density, $\times 10^6$ tracks cm^{-2}			Age Dispersion $P\chi^2$	Central Age $\pm 2\sigma$, Ma	Apatite Mean Track Length, $\mu m \pm 1$ SE (Number of Tracks)	Standard Deviation, μm
						ρ_s (N_s)	ρ_i (N_i)	ρ_d (N_d)				
THT1	1450	Esenyurt 39°02′03″N; 28°46′04″E	Quartzite (Çine)	apatite	19	0.1210 (71)	1.225 (719)	1.198 (8270)	0.46% (71.4%)	21.2 ± 5.5	14.43 ± 0.16 (29)	0.85
				zircon	20	1.449 (1277)	1.615 (1423)	0.4030 (5566)	<0.01% (95.3%)	23.6 ± 2.2	–	–
THT2	1210	S. Simav 39°04′57″N; 28°57′21″E	Leucogranite (Çine)	apatite	18	0.5676 (272)	6.934 (3323)	1.190 (8216)	<0.01% (99.0%)	17.5 ± 2.6	14.51 ± 0.10 (100)	1.04
THT3	1440	S.Simav 39°05′03″N; 28°55′57″E	Mica Schist (Çine)	apatite	20	0.7846 (623)	9.621 (7640)	1.182 (8162)	<0.01% (98.5%)	17.3 ± 2.0	14.78 ± 0.15 (100)	1.52
				zircon	20	2.843 (2540)	3.555 (3176)	0.4035 (5572)	<0.01% (98.0%	21.1 ± 1.5	–	–
THT4	1040	S. Simav 39°05′04″N; 28°58′02″E	Mica Schist (Çine)	apatite	20	0.2263 (220)	3.052 (2967)	1.174 (8108)	<0.01% (98.6%)	15.6 ± 2.5	14.56 ± 0.10 (100)	0.99
				zircon	14	9.264 (2917)	12.15 (3824)	0.4040 (5579)	2.61% (30.8%)	20.1 ± 1.4	–	–
THT5	925	S. Simav 39°05′23″N; 28°57′42″E	Leucogranite (Çine)	apatite	20	0.7776 (378)	11.58 (5627)	1.166 (8054)	<0.01% (99.9%)	14.0 ± 1.8	14.39 ± 0.14 (100)	1.37
				zircon	20	2.334 (1444)	3.092 (1913)	0.4044 (5585)	1.75% (67.2%)	19.9 ± 1.7	–	–
THT6	1060	Eynal 39°07′57″N; 29°01′37″E	Schist (Çine)	apatite	3	0.2599 (14)	3.064 (165)	1.159 (8000)	<0.01% (18.0%)	17.6 ± 9.9	14.97 ± 0.28 (7)	0.68
				zircon	20	3.760 (1594)	4.762 (2019)	0.4049 (5592)	<0.01% (96.4%)	20.9 ± 1.8	–	–
THT7	1480	Gölcük Dagi 39°09′38″N; 29°05′16″E	Granite (Egrigöz)	apatite	20	0.1224 (61)	1.691 (843)	1.151 (7945)	0.01% (97.6%)	14.9 ± 4.1	14.88 ± 0.09 (100)	0.88
				zircon	20	2.998 (2389)	3.870 (3084)	0.4054 (5598)	5.22% (25.4%)	20.5 ± 1.5	–	–
THT8	970	Hisarcik 39°16′15″N; 29°08′51″E	Granite (Egrigöz)	apatite	20	0.0770 (49)	1.133 (721)	1.143 (7891)	0.02% (93.8%)	13.9 ± 4.2	14.57 ± 0.11 (100)	1.09
				zircon	20	3.201 (2913)	4.040 (3677)	0.4058 (5605)	5.46% (19.4%)	21.0 ± 1.5	–	–
THT9	1250	Hisarcik 39°17′47″N; 29°05′00″E	Granite (Egrigöz)	apatite	20	0.1675 (99)	2.289 (1353)	1.135 (7837)	0.03% (94.5%)	14.9 ± 3.3	14.61 ± 0.13 (100)	1.28
				zircon	20	4.097 (2857)	5.034 (3511)	0.4063 (5611)	0.62% (54.9%)	21.6 ± 1.5	–	–
THT10	1500	Hisarcik 39°20′37″N; 29°04′30″E	Granite (Egrigöz)	apatite	20	0.1578 (85)	2.254 (1214)	1.127 (7783)	<0.01% (99.9%)	14.1 ± 3.3	14.59 ± 0.12 (100)	1.18
				zircon	20	3.476 (3000)	4.368 (3770)	0.4068 (5618)	0.01% (85.0%)	21.1 ± 1.5	–	–
THT11	1260	Darici 39°16′05″N; 29°02′53″E	Granite (Egrigöz)	apatite	20	0.1445 (96)	1.885 (1252)	1.119 (7729)	<0.01% (99.9%)	15.4 ± 3.5	14.68 ± 0.08 (100)	0.84
				zircon	20	4.266 (3022)	5.041 (3571)	0.4072 (5624)	2.10% (39.4%)	22.5 ± 1.6	–	–
THT12	880	Aydinlar 39°30′14″N; 29°01′30″E	Flysch (Izmir/Ankara)	apatite	10	0.0840 (34)	0.3139 (127)	1.112 (7675)	<0.01% (97.9%)	53.2 ± 20.9	14.79 ± 0.37 (8)	0.97
THT14	1140	Dagardi 39°27′38″N; 29°00′31″E	Flysch (Izmir/Ankara)	apatite	18	1.236 (384)	6.420 (1995)	1.326 (9154)	0.73% (60.9%)	45.6 ± 6.1	13.29 ± 0.21 (100)	2.07

Table 1. (continued)

Sample	Elevation, m	Location (WGS84) (Rock Type)	Rock Type (Unit/Nappe)	Mineral	Number of Crystals	Track Density, $\times 10^6$ tracks cm^{-2} ρ_s (N_s)	ρ_i (N_i)	ρ_d (N_d)	Age Dispersion $P\chi^2$	Central Age ±2σ, Ma	Apatite Mean Track Length, μm ± 1 SE (Number of Tracks)	Standard Deviation, μm
				zircon	20	14.68 (5088)	1.685 (584)	0.4077 (5630)	<0.01% (97.9%)	228.0 ± 23.0	–	–
THT15	1340	Ihlamur 39°23′43″N; 29°02′23″E	Granite (Egrigöz)	apatite	20	0.0970 (71)	1.784 (1306)	1.320 (9112)	<0.01% (98.6%)	12.9 ± 3.3	14.79 ± 0.09 (100)	0.89
				zircon	20	3.427 (2319)	4.119 (2787)	0.4082 (5637)	<0.01% (95.8%)	22.2 ± 1.5	–	–
THT16	1160	Esenbag 39°23′17″N; 29°01′37″E	Granite (Egrigöz)	apatite	20	0.0967 (72)	1.548 (1152)	1.313 (9070)	<0.01% (99.8%)	14.7 ± 3.7	15.04 ± 0.10 (69)	0.84
				zircon	20	3.296 (2886)	4.114 (3602)	0.4086 (5643)	<0.01% (94.8%)	21.4 ± 1.5	–	–
THT17	790	Harmancik 39°17′14″N; 28°58′28″E	Gran. Mylonite (?Çine)	apatite	20	0.2704 (230)	2.891 (2459)	1.307 (9027)	<0.01% (99.9%)	21.9 ± 3.4	14.88 ± 0.10 (100)	0.99
				zircon	20	6.035 (4084)	7.203 (4874)	0.4091 (5650)	4.81% (21.7%)	22.5 ± 1.5	–	–
THT18	690	Külcü 39°21′36″N; 28°58′05″E	Pegmatite (?Triassic)	apatite	17	1.011 (395)	11.02 (4305)	1.301 (8985)	<0.01% (99.9%	21.4 ± 2.7	14.28 ± 0.09 (100)	0.88
THT19	850	A. Yavu 39°18′26″N; 28°57′05″E	Granite (Koyanuba)	apatite	20	0.2104 (190)	2.041 (1843)	1.295 (8943)	<0.01% (99.4%)	23.9 ± 4.0	14.62 ± 0.10 (100)	0.99
				zircon	20	5.953 (3543)	6.549 (3898)	0.4096 (5656)	4.51% (15.4%)	24.2 ± 1.7	–	–
THT20	1280	Koyunoba 39°13′28″N; 28°52′51″E	Granite (Koyanuba)	apatite	8	0.5021 (95)	4.271 (808)	1.289 (8900)	<0.01% (96.7%)	27.1 ± 6.2	14.91 ± 0.24 (21)	1.06
				zircon	20	2.908 (1831)	3.279 (2065)	0.4100 (5663)	1.88% (53.9%)	23.7 ± 1.9	–	–
THT21	1210	Koyunoba 39°12′50″N; 28°53′50″E	Granite Boudin (Çine)	apatite	20	0.9010 (382)	9.027 (3827)	1.283 (8858)	<0.01% (92.7%)	22.9 ± 3.0	14.77 ± 0.09 (100)	0.91
				zircon	20	3.991 (1808)	4.515 (2045)	0.4105 (5669)	0.01% (95.9%)	23.7 ± 1.9	–	–
THT22	900	Efir 39°11′55″N; 28°48′30″E	Granite (Koyanuba)	apatite	20	0.2647 (253)	2.032 (1942)	1.277 (8816)	4.09% (41.9%)	29.8 ± 4.5	14.69 ± 0.11 (100)	1.13
				zircon	20	6.664 (3405)	6.196 (3166)	0.4110 (5676)	0.49% (53.4%)	28.8 ± 2.0	–	–
THT23	900	E. Simav 39°05′24″N; 29°02′40″E	Granite (Egrigöz)	apatite	20	0.1602 (94)	1.801 (1057)	1.271 (8773)	<0.01 (99.9%)	20.3 ± 4.6	14.62 ± 0.10 (100)	1.02
				zircon	20	4.014 (2866)	4.713 (3365)	0.4114 (5682)	0.28% (67.5%)	22.9 ± 1.6	–	–
THT24	600	E. Selendi 38°42′50″N; 28°55′32″E	Augen Gneiss (Çine)	apatite	20	0.3744 (257)	5.217 (3581)	1.264 (8731)	0.01% (94.3%)	16.3 ± 2.4	14.25 ± 0.11 (100)	1.08
				zircon	20	2.829 (2051)	3.187 (2311)	0.4119 (5689)	0.01% (88.7%)	23.9 ± 1.9	–	–
THT25	510	Yenisehir 38°40′11″N; 29°01′11″E	Leucogranite (Çine?)	apatite	8	0.3809 (81)	8.577 (1824)	1.258 (8688)	<0.01% (84.3%)	10.0 ± 2.4	13.06 ± 0.14 (100)	1.38
THT26	300	Kula 38°26′45″N; 28°31′55″E	Mica Schist (Çine)	apatite	20	0.1353 (60)	1.760 (780)	1.252 (8646)	<0.01% (99.1%)	17.3 ± 4.8	14.08 ± 0.26 (10)	0.77
				zircon	9	1.700 (622)	1.872 (685)	0.4124 (5695)	<0.01% (90.4%)	24.4 ± 3.0	–	–

Table 1. (continued)

Sample	Elevation, m	Location (WGS84) (Rock Type)	Rock Type (Unit/Nappe)	Mineral	Number of Crystals	Track Density, $\times 10^6$ tracks cm^{-2}			Age Dispersion $P\chi^2$	Central Age $\pm 2\sigma$, Ma	Apatite Mean Track Length, $\mu m \pm 1$ SE (Number of Tracks)	Standard Deviation, μm
						ρ_s (N_s)	ρ_i (N_i)	ρ_d (N_d)				
THT27	350	Killik 38°23′47″N; 28°38′32″E	Granite (Triassic)	apatite	9	0.1007 (47)	1.382 (645)	1.246 (8604)	<0.01% (89.4%)	16.3 ± 5.1	14.47 ± 0.11 (3)	1.56
				zircon	17	4.870 (1271)	5.322 (1389)	0.4128 (5701)	<0.01% (99.9%)	24.6 ± 2.3	–	–

[a]Notes are (1) analyses by external detector method using 0.5 for the $4\pi/2\pi$ geometry correction factor; (2) ages calculated using dosimeter glass: CN5 with $\zeta_{CN5} = 358.8 \pm 12.7$; CN2 with $\zeta_{CN2} = 130.7 \pm 2.8$; and (3) $P\chi^2$ is the probability of obtaining a χ^2 value for v degrees of freedom where ν = number of crystals − 1;

suspect the presence of excess He generated from submicroscopic U- and/or Th-rich inclusions [e.g., *Ehlers and Farley*, 2003]. Both analyses from sample THT3 are the same within error (17.8 ± 1.1 and 17.9 ± 1.1 Ma) providing added confidence in the AHe age of this sample. For the purposes of this study we quote the age from sample THT3A, owing to its smaller Ft correction and higher yield of radiogenic ^{4}He. The 11 analytically acceptable sample AHe ages from the footwall vary between 8.0 ± 0.5 and 22.3 ± 1.3 Ma, while the only AHe age from the hanging wall of the SDF gives an age of 19.3 ± 1.2 Ma.

5. Data Interpretation

[21] The true extensional nature of a tectonic contact such as the SDF can only be suitably verified by a contrasting pressure- and/or temperature-time history from the footwall and hanging wall of the fault. *Wheeler and Butler* [1994] emphasize that kinematic shear sense indicators and the observation of low-pressure rocks overlying high-pressure rocks, without additional chronologic information, are insufficient criteria to diagnose crustal extension. This latter statement is particularly true in the Anatolide orogen where many of the tectonic contacts have been later tilted and folded, where out-of-sequence thrusts have been identified (such as the Eocene Cyclades-Menderes thrust) that juxtapose high- and low-pressure rocks of varying age, and where extensional reactivation of older thrust faults may have occurred. The acquisition of thermochronologic data allows constraints to be made on the timing and amounts of extension, particularly if other criteria such as offset geologic markers, and kinematic, stratigraphic, or metamorphic data are lacking or ambiguous.

5.1. Comparison of Hanging Wall and Footwall Thermal History

[22] A comparison of the time-temperature history of the hanging wall and footwall of the Simav detachment is presented in Figure 3. The low-temperature AFT, ZFT and AHe thermochronologic ages obtained in this study are plotted as time-temperature points using the closure temperatures assigned earlier for each system (70°C for AHe; 110 ± 10°C for AFT; and 280 ± 30°C for ZFT) and the determined mineral age. The cooling path of the footwall is further constrained by a biotite ^{40}Ar/^{39}Ar age of 20.2 ± 0.3 Ma (sample 98/2 in Figure 2a) from the Eğrigöz granite published by *Işik et al.* [2004], a muscovite ^{40}Ar/^{39}Ar age of 24.7 ± 1.2 Ma from the southern part of the Gördes massif (sample 93T9 in Figure 2a [*Ring et al.*, 2003a]), and U-Pb SIMS ages of 24.4 ± 0.3 Ma from a leucogranitic dike south of Simav (sample THT 5) and 20.7 ± 0.6 Ma from the Eğrigöz granite (sample THT7) obtained by *Ring and Collins* [2005]. We apply a minimum crystallization temperature of 700°C for magmatic zircon growth at the time of granite intrusion [*Ring and Collins*, 2005]. We also assign closure temperatures of ~310°–380°C for Ar in biotite and 350°–430°C for Ar in muscovite in the cooling granites [e.g., *Lister and Baldwin*, 1996], although these values are not critical to our interpretation.

Table 2. Apatite (U-Th)/He Data[a]

Sample	Latitude (WGS84)	Longitude (WGS84)	Elevation, m	Corrected Age, Ma	±2σ, Ma	Raw Age, Ma	±1σ, Ma	Ft	Number of Grains	Mass, μg	MWAR, μm	U, ppm	Th, ppm	Th/U	He, ncc
THT1A	39.03417	28.76778	1450	795.11	42.66	563.73	30.24	0.709	1	2.05	46.0	9.378	0.956	0.1019	1.4137
THT3A	39.08417	28.93250	1440	17.82	1.07	13.24	0.28	0.743	2	6.80	50.9	113.164	5.427	0.0480	1.2453
THT3B	39.08417	28.93250	1440	17.97	1.08	12.24	0.28	0.680	1	1.73	39.8	131.130	5.106	0.0399	0.3389
THT5A	39.08972	28.96167	925	8.02	0.48	5.87	0.12	0.732	2	5.86	49.2	174.905	1.756	0.0100	0.7279
THT7A	39.16056	29.08778	1480	27.90	1.67	17.44	0.32	0.625	3	3.99	34.1	15.317	39.640	2.5880	0.2079
THT7B	39.16056	29.08778	1480	21.88	1.31	14.77	0.32	0.675	1	1.91	40.8	14.849	36.807	2.4788	0.0804
THT8A	39.27083	29.14750	970	18.12	1.09	12.67	0.23	0.699	3	8.69	42.7	15.679	33.410	2.1308	0.3140
THT8B	39.27083	29.14750	970	13.29	0.80	8.47	0.23	0.637	1	1.40	35.8	10.959	29.398	2.6825	0.0257
THT10A	39.34361	29.07500	1500	21.56	1.29	13.32	0.30	0.618	1	1.15	33.5	30.217	65.426	2.1652	0.0847
THT14A	39.46056	29.00861	1140	19.31	1.16	12.82	0.24	0.664	2	3.25	40.1	40.056	69.066	1.7242	0.2843
THT15A	39.39528	29.03972	1340	19.21	1.15	13.62	0.25	0.709	3	7.12	47.5	16.414	31.773	1.9357	0.2807
THT15B	39.39528	29.03972	1340	40.27	2.42	27.87	0.52	0.692	1	2.18	44.8	26.030	87.741	3.3708	0.3443
THT19A	39.30722	28.95139	850	15.97	0.96	11.57	0.22	0.724	3	8.86	48.0	22.724	17.717	0.7797	0.3334
THT21A	39.21389	28.89722	1210	22.31	1.34	17.40	0.37	0.780	1	4.66	64.5	89.728	2.973	0.0331	0.8864
THT22A	39.19861	28.80833	900	18.02	1.08	14.26	0.27	0.791	2	14.14	65.1	26.431	24.935	0.9434	0.7880
THT23A	39.09000	29.04444	900	10.37	0.62	7.27	0.14	0.701	3	7.78	44.9	9.595	25.178	2.6242	0.1063

[a]MWAR is the mass-weighted average radius and Ft is the alpha-ejection correction.

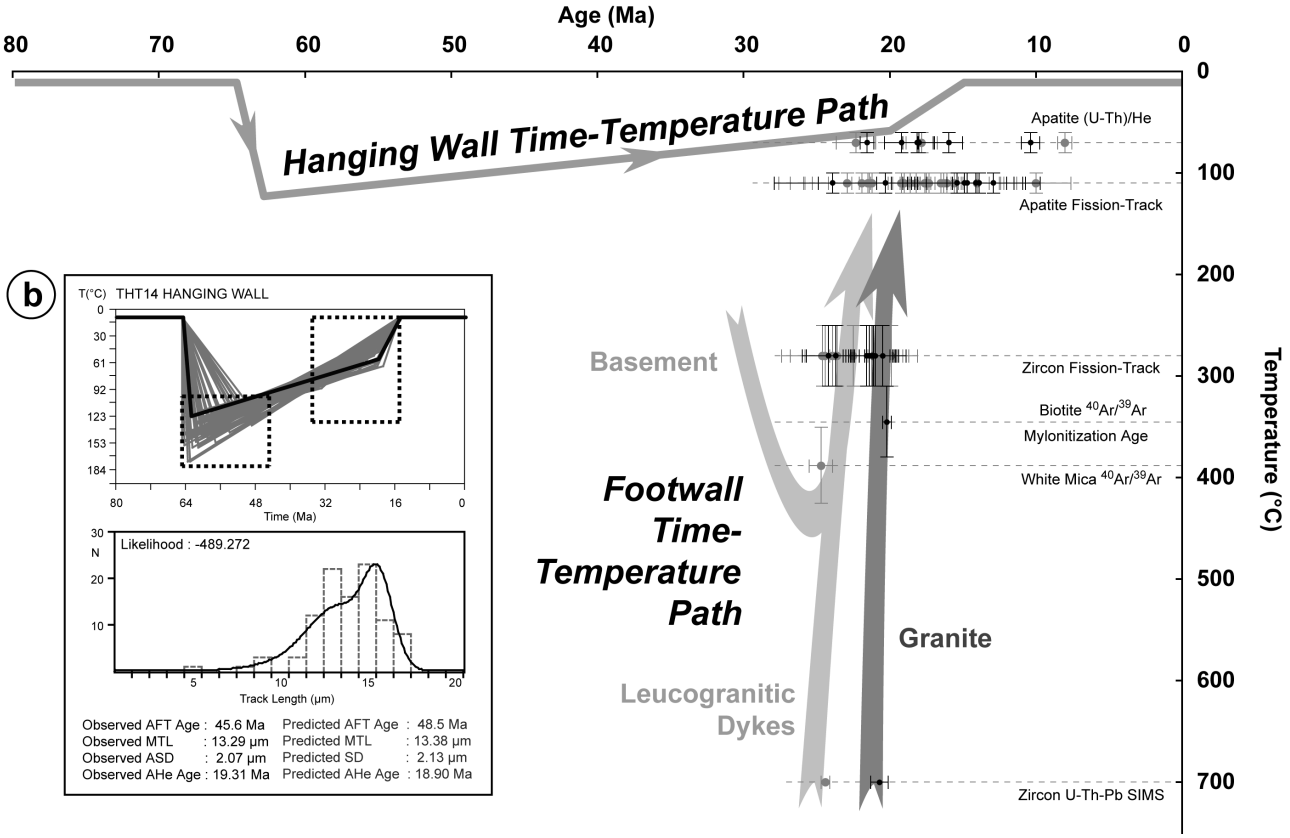

Figure 3. (a) Time-temperature plot illustrating the contrasting thermal history of the hanging wall and footwall of the Simav detachment fault. (b) Hanging wall thermal history based on the thermal history that best predicted the observed apatite fission track data from sample THT14 (see text for details). Although the footwall basement rocks yield $^{40}Ar/^{39}Ar$ white-mica cooling age of 24.7 ± 1.2 Ma and have been mylonitized close to the detachment [*Ring and Collins*, 2005], their lack of pervasive metamorphic overprint implies that they were at temperatures close to ~400°C at the time of dike intrusion.

[23] The cooling histories of the hanging wall and footwall of the SDF are very different. The footwall underwent very rapid cooling between about 25 and 18 Ma, well after the rocks in the hanging wall had cooled to temperatures below 110 ± 10°C. This juxtaposition of rocks with old cooling ages in the hanging wall against rocks with younger ages in the footwall is consistent with extensional offset [*Wheeler and Butler*, 1994; *Thomson*, 1998]. The interpretation of cooling in the footwall is complicated by the presence of the synkinematic Miocene Eğrigöz and Koyunoba plutons that dominate the northernmost part of the SDF footwall. The intrusion ages of these plutons are concordant within error of the ZFT ages, most of the AFT ages, and even some of the AHe ages, indicating very rapid cooling from >700°C to near surface temperatures (<∼70°C) within at most a few million years between about 21 and 18 Ma (early Miocene). *Ring and Collins* [2005] suggest that such rapid cooling indicates a very shallow intrusion depth during the latter stages of movement along the SDF. Away from the thermal influence of these plutons, particularly south of Simav town, the thermochronologic data from the footwall of the SDF indicate slightly slower, but still rapid cooling between about 25 Ma and ∼18 ± 1 Ma at rates of between 25 and 50°C/m.y, consistent with similar rates based on the reconnaissance data presented by *Ring et al.* [2003a] from the south part of the Gördes submassif. Note that although the crystallization temperature of the intruding leucograntic dikes was high (>700°C), the nature of synkinematic deformation of the surrounding basement rocks into which the dikes intruded (i.e., feldspar-brittle, quartz-ductile) indicates that they were low greenschist facies conditions (∼300°–350°C) at the time of onset of accelerated cooling at ∼25 Ma [*Ring and Collins*, 2005].

[24] In contrast, the rocks of the hanging wall yield much older thermochronologic ages indicative of slow monotonic cooling in the uppermost parts of the crust since at least the Eocene. The 228 Ma ZFT age from the ophiolitic Bornova flysch is older than the presumed Late Cretaceous-Paleocene stratigraphic age of these rocks [*Okay and Siyako*, 1993], implying that these rocks have not seen temperatures high enough to significantly anneal fission tracks in zircon (>250 ± 20°C) since deposition. The AFT ages from the same rocks (especially the more precise THT14 age of 46 ± 6 Ma) are younger that the depositional age. These rocks must thus have been heated sufficiently since deposition to reset the AFT age before subsequently being slowly cooled through the apatite partial annealing zone to near surface temperatures sometime before deposition of the oldest unconformably overlying Neogene sedimentary deposits. This is better demonstrated in an AFT inverse time-temperature model using the approach of *Gallagher* [1995] and the apatite FT annealing model of *Laslett et al.* [1987]. The T-t path that best predicts the observed data requires rapid heating following deposition between about 65 and 50 Ma followed by near monotonic cooling from temperatures of ∼120°C between about 65 and 50 Ma to the surface (∼10°C) sometime before ∼15 Ma (Figure 3b) at a time-averaged cooling rate of ∼3°C/Myr The best fitting time-temperature paths also demonstrate that the rocks of the hanging wall to the SDF were below ∼110 ± 10°C (i.e., the upper 2–3 km of crust) since at least Eocene times.

[25] In contrast to the AFT ages, the AHe ages from both the hanging wall and footwall of the SDF are concordant within error (∼19 Ma). This is an important finding, as it requires that relative offset along the SDF must have all but ceased by this time. Both sides of the fault and the fault rocks themselves must have had a common cooling history from temperatures somewhere between the closure temperature of the AFT and AHe systems (i.e., between 110 ± 10°C and ∼70°C) between ∼19 Ma and the age of the oldest sediments deposited on the fault (∼15 Ma) [*Ercan et al.*, 1997]. Furthermore, as much as 2–3 km of overburden must have been removed (the exact amount being dependent on the assumed geothermal gradient) from the current exposure level of the fault at its northernmost outcrop since the SDF became inactive. The 19 Ma AHe age from the hanging wall is consistent with the monotonic post-Eocene cooling history of the hanging wall rocks that best predicts the observed AFT data. According to the He diffusion model and parameters derived by *Farley* [2000] for Durango apatite (E_a = 33 kcal/mol; D_0 = 31.6 cm^2/s), the best fit time-temperature history in Figure 3b predicts an AHe age of 18.9 Ma for a 60 μm diameter apatite grain, within 1σ error of the observed AHe age of 19.3 Ma.

[26] An alternative explanation for the young AHe age in the hanging wall is that it was thermally reset by the transfer of heat from the footwall into the hanging wall close to the fault, either by the juxtaposition of hot footwall rocks against a colder hanging wall, or from the local thermal effects of intrusion of the synkinematic ∼21 Ma Eğrigöz pluton [e.g., *Kounov et al.*, 2004]. This heating effect, must, however, have been minimal; sufficient to reset the AHe age (>∼70°C), but insufficient to significantly effect the AFT ages (<110 ± 10°C). However, at such temperatures, at least a partial resetting of the AFT system would be expected. Sedimentary rocks, like those sampled from the hanging wall, would be likely to contain a diverse population of apatite grains with highly variable annealing kinetics [e.g., *Carlson et al.*, 1999]. Partial resetting of such a sample should manifest itself in a wide spread of single grain apatite ages, but, no significant single grain age variation is seen in samples THT12 and 14. The narrow age dispersion is more consistent with the samples having cooled monotonically at a moderate rate through the AFT partial annealing zone.

[27] However, either of these alternative explanations for the young AHe age in the hanging wall of the SDF does not alter our main finding; namely that the contrast in hanging wall and footwall cooling histories is consistent with the SDF have acted as an extensional tectonic contact, with rapid footwall cooling and unroofing, sometime between ∼25 and ∼19 Ma, with relative offset having ceased by ∼19 Ma.

5.2. Footwall Age Versus Slip Direction Profile

[28] Low-temperature thermochronologic ages from sample profiles along the slip direction of major detachment faults have been used as an interpretative tool in numerous

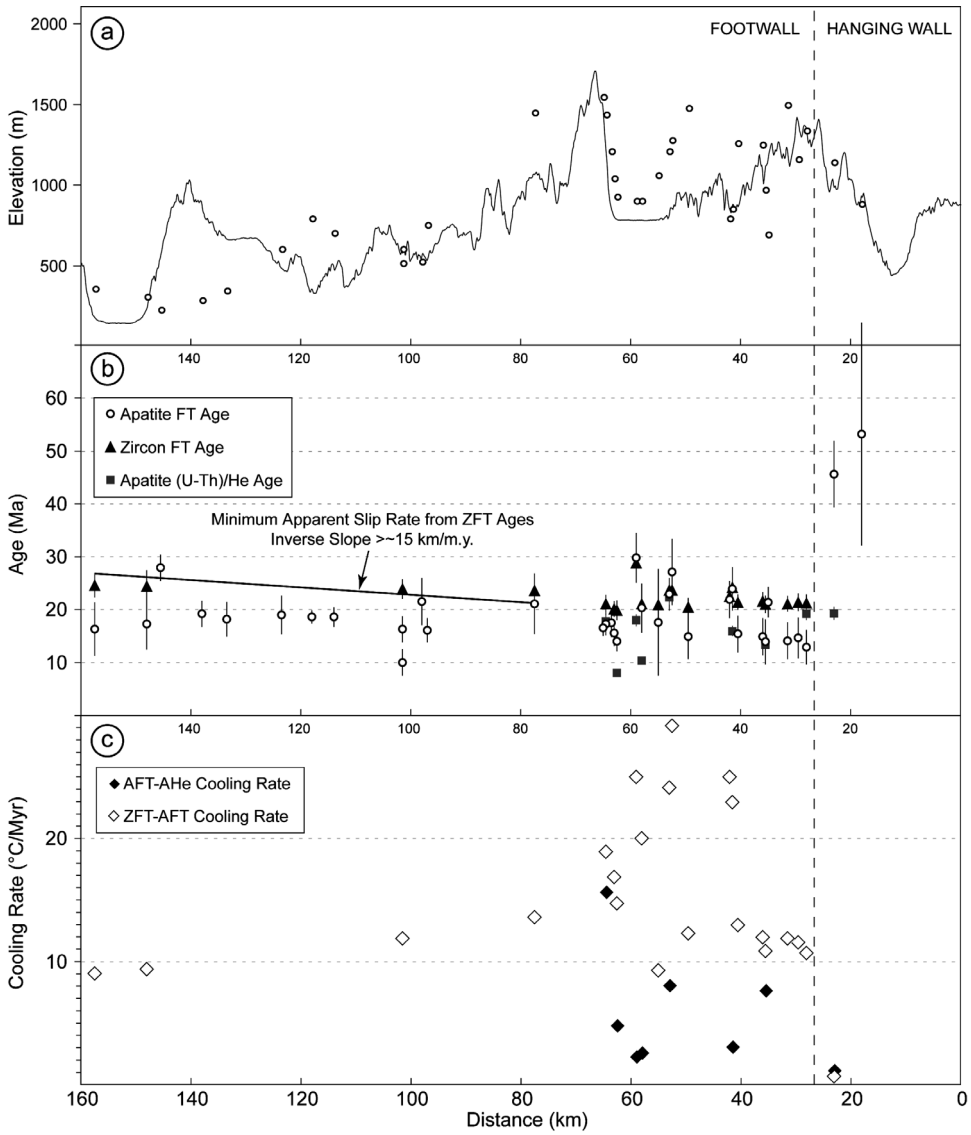

Figure 4. (a) NNE-SSW linear topographic profile (A-A′ from Figure 2) approximately parallel to top-to-the-NNE hanging wall slip on the SDF showing location and elevation of samples points projected perpendicularly onto profile plane. The approximate position of the northern most surface outcrop of the SDF is also shown. All samples taken to the SSW of the point are from the footwall; those to the NNE are all from the hanging wall. (b) Plot of different thermochronologic ages versus distance in fault slip direction. The minimum apparent slip rate is based on four zircon FT ages given their 2σ error. Note the invariance in apatite FT ages ($\sim$18 Ma) across the whole length of exposed footwall of the SDF and that these ages are consistently $\sim 2-5$ Ma younger than the zircon FT ages. The footwall ages to the NNE of the 70 km marker are largely taken from (or reset by) the $\sim$21 Ma Eğrigöz and Koyunoba plutons. (c) Plot of cooling rates from those samples where an age from more than one different chronometer were obtained. Time-averaged cooling rates were derived by dividing the difference in respective closure temperatures by the difference in age (70°C for AHe, 110°C for AFT, and 280°C for ZFT). Note that most samples show a slow down in cooling rates below the closure temperature of the AFT system.

metamorphic core complexes to quantify characteristics such as the slip rate, minimum displacement, time of onset of slip, and initial fault plane dip angle [see *Foster and John*, 1999, and references therein]. This approach has proven particularly valuable where stratigraphic or other geologic markers are absent, or where rocks either side of a detachment represents units formerly juxtaposed by an earlier out-of-sequence thrust, such as is the case with the SDF and the earlier Cyclades-Menderes thrust.

[29] Figure 4 shows the relationship of ZFT, AFT and AHe ages with distance in the top-to-the-NNE slip direction of the SDF. Each data point is projected onto the NNE-SSW

linear profile shown in Figure 2b; hence some of the points on the topographic profile (Figure 4a) do not plot directly on the topography of the profile itself. The most striking feature of this plot is that both the ZFT and AFT ages show little or no variation in age in the direction of slip along the entire ~130 km length of the presumed footwall of the SDF. The uniform ~24–20 Ma ZFT ages from the Miocene plutonic rocks in the northern part of the footwall are all within 2σ error of the ~21 Ma intrusion age [*Ring and Collins*, 2005]. One exception is sample THT 22. This yields a slightly older ZFT age of 29 ± 2 Ma (and similarly old AFT age of 30 ± 5 Ma). The reason for these two older ages is unclear. Possible explanations are that they could represent either an older partially reset Triassic granite from part of the hanging wall, or an older part of the Koyunoba pluton. In addition, both the apatite and zircon from this sample were of poor quality, with many inclusions and track-like dislocations. Excess spontaneous tracks could thus have been counted leading to overestimation of the true fission track age. Otherwise, the concordance of the other ZFT ages with the age of intrusion confirms that these rocks cooled very rapidly following their synkinematic emplacement. The thermal influence of Miocene plutonism also reset the ZFT ages in the surrounding country rocks from the northern part of the exposed SDF footwall, thus destroying any former trend of decreasing age in the hanging wall slip direction that may have existed prior to plutonism to allow estimation of slip rate. The four ZFT ages from the Gördes submassif south of Simav are older (between 24.6 ± 2.2 and 23.6 ± 2.2 Ma) than the age of the Eğrigöz pluton, but are still invariant over a distance of ~80 km in the slip direction. The distance between these sample ages (within 2σ error) implies a slip rate of at least ~15 km/Myr, assuming the cooling ages were related to the removal of the hanging wall by top-to-the-NNE detachment faulting and that isotherms were static (i.e., had reached a steady state following the onset of detachment faulting [see *Ketcham*, 1996]). Note, however, that if regional erosion occurred contemporaneously with footwall slip, then this calculated slip rate would be lower, and dependent on the angle of fault dip. For example for a background vertical erosion (denudation) rate of 0.5 mm/yr, a slip rate of between 7 and 15 km/Myr, and a fault dip of 30°, then the slip rate will be overestimated by ~7 to 15%. The lower the angle of dip of the fault, then the larger the overestimate will be. The total time of fault activity between ~25 and ~19 Ma and an approximate time-averaged slip rate of ~15 km/Myr imply a very high offset, possibly as much as ~90 km, similar to the present horizontal distance between these samples. A fast slipping detachment interpretation is consistent with the muscovite $^{40}Ar/^{39}Ar$ cooling age of 24.7 ± 1.2 Ma from the south part of the Gördes massif (sample 93T9 in Figure 2a [*Ring et al.*, 2003a]) and an $^{40}Ar/^{39}Ar$ age of 22.9 ± 0.5 Ma from syntectonic mica porphyroclasts (mica fish) within a mylonite south of the Koyunoba granite (sample 98/1 of *Işik et al.* [2004], location shown in Figure 2a). Furthermore, as quartz-ductile deformation has been demonstrated to occur at temperatures higher than the ZFT closure temperature [*Brix et al.*, 2002], footwall ductile deformation and mylonitization along the southern exposed segments of the SDF away from the influence of early Miocene plutonism must have ceased sometime before ~23.6 ± 2.2 Ma. The ductile deformation of the Eğrigöz and Koyunoba granites during their emplacement at ~21–20 Ma farther north [*Ring and Collins*, 2005] suggests that the active ductile deforming part of the SDF migrated northward with time.

[30] A similarly large displacement of >100 km has been proposed to explain the coeval late Oligocene-early Miocene exhumation of HP-LT rocks in the footwall of the Cretan detachment to the west of the SDF [*Ring et al.*, 2001b]. However, such slip rates and total displacements are higher than those recognized in the Aegean (with slip rates 6–9 km/Myr and total offsets of between 12 and 70 km [*Ring et al.*, 2003b; *Kumerics et al.*, 2005; *Brichau et al.*, 2006] and the maximum total offset recognized in the Basin and Range province (~55 km for the Harcuvar Mountains metamorphic core complex [*Reynolds and Spencer*, 1985; *Carter et al.*, 2004]). The lack of Anatolide orogen or later HP-LT rocks in footwall of the SDF implies that the SDF did not exhume rocks from significant depths and hence must have had a low angle of dip while active, despite the apparently large total amount of slip and high slip rates [e.g., *Ring et al.*, 2003b].

[31] An alternative explanation for almost uniform ZFT ages over ~80 km in the slip direction is that they record cooling by thermal relaxation (in situ lowering of the geothermal gradient) following regional resetting during a highly elevated geothermal gradient related to the widespread intrusion of leucogranitic dikes at ~25–24 Ma throughout the Gördes submassif [*Ring and Collins*, 2005]. However, the continuation of large-scale footwall magmatism in the Miocene suggests that such a significant cool down is unlikely.

[32] The AFT ages are invariant in the direction of hanging wall slip, and importantly are almost always significantly younger (~2–5 Ma) than ZFT ages from the same sample. All the AFT ages, with the exception of sample T68 of *Ring et al.* [2003a] and sample THT25 of this study, overlap within 2σ error, with a weighted mean age of 18.2 ± 0.7 ($P\chi^2$ = >99%). If the AFT ages were related to fast cooling associated with rapid unroofing by detachment faulting, then near concordant ZFT and AFT ages would be expected [e.g., *Foster and John*, 1999]. Instead, the similarity in AFT ages across the ~130 km swath of the SDF footwall implies a more widespread regional cooling between about 19 and 17 Ma, after motion on the presumed SDF had ceased. We note also that the SDF slip rate of ~10 km/Myr between about 19 and 17 Ma estimated by *Ring et al.* [2003a] from an apparent inverse slope of reconnaissance AFT ages with distance in the slip direction is not supported by the new AFT and ZFT data of this study. The timing of slip proposed by *Ring et al.* [2003a] is also inconsistent with the ~21 Ma age of synmagmatic extensional kinematics in the northern part of the footwall [*Ring and Collins*, 2005], and apparent cessation of fault slip shortly thereafter. The older ~27 Ma AFT age published by *Ring et al.* [2003a] from the

southernmost part of the Gördes submassif close to the Büyük Menderes Graben (Figure 2) indicates the presence of an exhumed partial AFT annealing zone in the footwall. This implies that the surface breakaway fault of the main Simav detachment was situated slightly farther south, but has been subsequently removed by later Miocene to Pliocene erosion across the entire Anatolide orogen [*Ring et al.*, 2003a]. The position of this breakaway fault is consistent with our ~90 km estimate for the total extensional offset along the SDF. *Seyitoğlu et al.* [2004] on the other hand propose that the SDF breakaway fault is situated much farther south, intercepting the surface at the southern boundary of the Kale-Tavas basin at the southern margin of the Anatolide orogen. This would require an orogen scale extremely low-angle or subhorizontal detachment fault over 150 km long.

[33] Where ages from two (or more) thermochronologic systems were obtained from the same sample, time averaged cooling rates were derived by dividing the difference in respective closure temperatures by the difference in age (Figure 4c). ZFT and AFT cooling ages from the SDF footwall of the Gördes submassif south of Simav indicate that the regionally extensive cooling between about 24 and 17 Ma (away from the thermal influence of Miocene plutonism) occurred at an average rate of 10–20°C/Myr. This rate and the regional extent of this cooling appear to better support a phase of relatively rapid erosional denudation. The alternative possibility of unroofing linked to major detachment faulting typically results in much higher rates of footwall cooling (25–>75°C in the Aegean [*Ring et al.*, 2003b; *Brichau et al.*, 2006; *Kumerics et al.*, 2005] and >40°C-100°C in the Colorado River extensional corridor [*Foster and John*, 1999]). Rapid regional postdetachment erosion of the Gördes submassif may have been aided by the easy erodibility of the hanging wall rocks. These are still preserved today as isolated klippen, and comprise very tectonically disturbed and unconsolidated ophiolitic flysch. The underlying footwall rocks, on the other hand, comprise more erosionally resistant mylonites and crystalline basement rocks. This would also help explain the apparent preservation of SDF footwall mylonites and the possible detachment surface itself identified below unconformably overlying Neogene sedimentary rocks of the Gördes and Selendi basins by *Purvis and Robertson* [2004a]. The presence of hanging wall klippen also indicates that little erosion of the footwall rocks has occurred. The minimum age for the end of this phase of erosion is constrained by a high-precision biotite $^{40}Ar/^{39}Ar$ age of 16.4 ± 0.1 Ma from tuffs within the Selendi and Gördes basins [*Purvis and Robertson*, 2004a]. This implies an increased rate of final cooling and hence denudation of the Gördes submassif (i.e., including both the footwall and hanging wall rocks of the SDF, and the SDF itself) from 110 ± 10°C at ~18 Ma, to surface temperatures at ~16 Ma (an equivalent mean rate of ~50°C/Myr Finally, cooling from ~110 ± 10°C implies removal of ~2–3 km of overburden (obviously dependent of the assumed geothermal gradient, which given the presence of widespread magmatism at this time, was likely high) comprising largely rocks of the hanging wall after cessation of activity along the SDF at ~19 Ma, but before deposition of the Selendi and Gördes basins.

[34] Near concordant AFT ages along the footwall of the SDF could, alternatively reflect the resetting of ages by the influx of hot mineralizing fluids [*Carter et al.*, 2004]. However, no pervasive mineralization of the appropriate age has been described from the Gördes submassif. Mineralization that is present [*Özgür*, 2002] is restricted and localized to the younger Pliocene-Recent E-W trending high-angle normal faults of the Simav and Büyük Menderes grabens.

5.3. Footwall Age-Elevation Relationship

[35] An age-elevation relationship (AER) from the footwall of the SDF was obtained by collecting samples from the high-relief escarpment of the Pliocene to Recent Simav Graben fault (SGF) south of Simav town (Figure 5a). Interpretation of this profile is complicated by ~10 ± 5° tilt of the SGF footwall block down to the south since Pliocene times. To restore the pre-Pliocene relative vertical offset of the samples in the AER, the AFT and AHe ages are plotted relative to their perpendicular distance below the SDF (Figure 5b). This corrects for the ~10 ± 5° tilt by assuming that the SDF was close to horizontal shortly after movement ceased at ~19 Ma. In an alternative representation of the Simav AER (Figure 5c), the ZFT and AFT ages are normalized to the closure temperature of the AHe system (70°C) to produce a "pseudo" age-elevation plot in a manner described by *Reiners et al.* [2003]. The present-day depth of the 70°C isotherm is taken as −1600 m (assuming a mean elevation of 1.2 km, and the modern geothermal gradient of ~40°C/km [e.g., *Ilkışık*, 1995]). The assigned errors of the ZFT and AFT closure temperatures are converted on this plot to equivalent depths of ±400 m and ±1200 m, respectively.

[36] Although the elevation difference between the samples is small, and the profile is not truly vertical, the AFT ages are consistent with a moderately fast minimum time-averaged denudation rate of >115 m/Myr between ~20 and ~15 Ma (Figure 5a). The AER is complicated by the anomalously young AHe age of 8.0 ± 0.5 Ma from sample THT5 at the base of the profile. This age can be explained in several ways: (1) It could record accelerated denudation following a slow down or hiatus between ~16 and ~8 Ma (solid grey line in Figure 5c) represented by deposition of the Gördes and Selendi sedimentary basins; (2) the young AHe is close to the SGF, and could reflect resetting or partial resetting related to hot fluids and epithermal mineralization found associated with many of the Pliocene-Recent E-W trending graben bounding faults in western Anatolia [*Özgür*, 2002] (dotted grey line in Figure 5c). This possibility is supported by a similar anomalously young AHe age of 10.4 ± 0.6 Ma (THT23) found close to the SDF, on the hanging wall side; or (3) the younger AHe age could represent the upper part of an exhumed fossil He partial retention zone (HePRZ), preserved following rapid footwall unroofing of the steeply dipping SGF since the late Pliocene. For example, both the AHe and AFT data from the AER are predicted well by a forward modeled HePRZ (and AFT partial annealing zone) produced by a time-tempera-

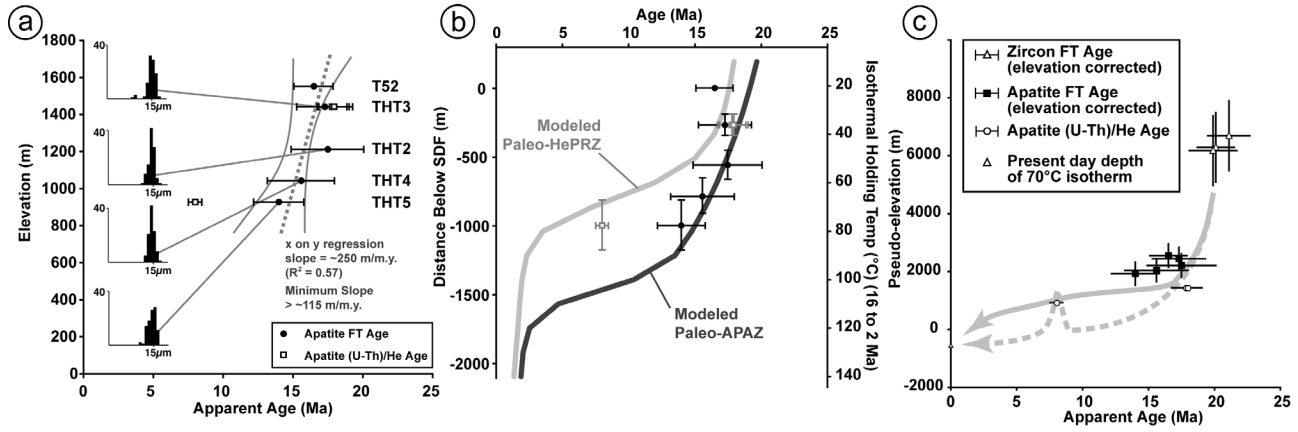

Figure 5. (a) AFT and AHe age-elevation relationship of samples taken from a high-relief section of the footwall of the Simav Graben fault (see Figure 2c). All samples have long mean track length distributions indicative of rapid cooling from 110 ± 10°C to below ~60°C. (b) Same age-elevation data as in Figure 5a but plotted relative to their perpendicular distance below the Simav detachment fault. The vertical error bars represent a ±5° variation in the postkinematic tilt of the fault. The two lines represent modeled paleoretention (or annealing) zones predicted by annealing and diffusion parameters and a thermal history detailed in section 5.3. (c) Pseudoage-elevation relationship where the elevation of ZFT and AFT ages and the present-day 70°C isotherm are normalized to the AHe system by assuming a present-day geothermal gradient of 40°C/km and a mean elevation of 1200 m). The two paths are possible alternative cooling histories to explain the anomalously young AHe age from the lowermost sample (THT5). See text for details.

ture history of rapid cooling at a rate of 40°C/Myr from temperatures >160°C before 16 Ma, isothermal holding between 16 and 2 Ma during sedimentation of the Selendi and Gördes basins, followed by final rapid denudation to the surface associated with footwall of SGF since 2 Ma (Figure 5b). The modeled HePRZ was produced using the diffusion model and parameters derived by *Farley* [2000] for Durango apatite assuming a grain size of 90 μm, close to the size of grains dated. The APAZ was produced using the *Laslett et al.* [1987] annealing model for Durango apatite. The latter interpretation requires that sample THT5 at the base of the profile was at a temperature of ~70°–80°C prior to final denudation in the last ~2 Myr. This would imply a relative offset on the SGF of 2–3 km, dependent on the transient geothermal gradient. This is compatible with a minimum 1 km offset of the SDF across the younger SGF implied by *Ring and Collins* [2005]. Note also that little removal of overburden is required from above the samples at the top of the profile since ~2 Ma, as according to the model, these samples were residing at near surface temperatures of ~20°–30°C before this time.

6. Tectonic Implications

[37] These new low-temperature thermochronologic constraints lead us to postulate that the Oligocene to early Miocene postcollision extensional SDF developed in a manner similar to that proposed for the Cenozoic development of the Snake Range décollement fault system in eastern Nevada, by *Miller et al.* [1999], modified after *Gans et al.* [1985] and *Rehrig and Reynolds* [1980]. These authors propose that previous crustal thickening helped initiate the development of a welt of hot crust leading to thermal weakening with localization and development of a detachment between a brittle deforming upper plate and ductile deforming lower plate. The brittle/ductile transition acts as a weak zone in which the detachments root [*Ring et al.*, 2003a, 2003b; *Kumerics et al.*, 2005]. Upper plate strain is distributed over a broad area, with high-angle normal faults rooting into the lower angle ductile deforming detachment interface. This ultimately drives renewed magmatism and extension resulting in doming and final uplift of the Snake Range and bending and tilting of the initial detachment horizon.

[38] In western Anatolia, Late Cretaceous to Eocene crustal thickening associated with the Anatolide orogen was superseded by widespread late Oligocene-early Miocene postcollision magmatism with a petrogenetic evolution consistent with an enriched asthenospheric mantle source suggestive of lithospheric delamination and asthenospheric upwelling [*Aldanmaz et al.*, 2000]. Similar models involving slab break-off, lithospheric delamination, combined with accelerated slab rollback have been invoked to explain comparable post-Eocene magmatism and postcollision or syncollision extension in the Aegean [e.g., *Zeilinga de Boer*, 1989; *Davies and von Blanckenburg*, 1995; *Thomson et al.*, 1999]. The coincidence in time of prekinematic and synkinematic leucogranitic dikes at ~24 Ma [*Ring and Collins*, 2005] with the onset of extension as recorded by the cooling history of the footwall of the SDF is remarkable. We postulate that this magmatic activity resulted in a transient increase in the geothermal gradient, resulting in thermal weakening and ductile low-angle extensional reactivation of the Eocene out-of-sequence Cyclades-Menderes thrust (Figures 6a–6d). *Axen* [1993] described similar low-angle

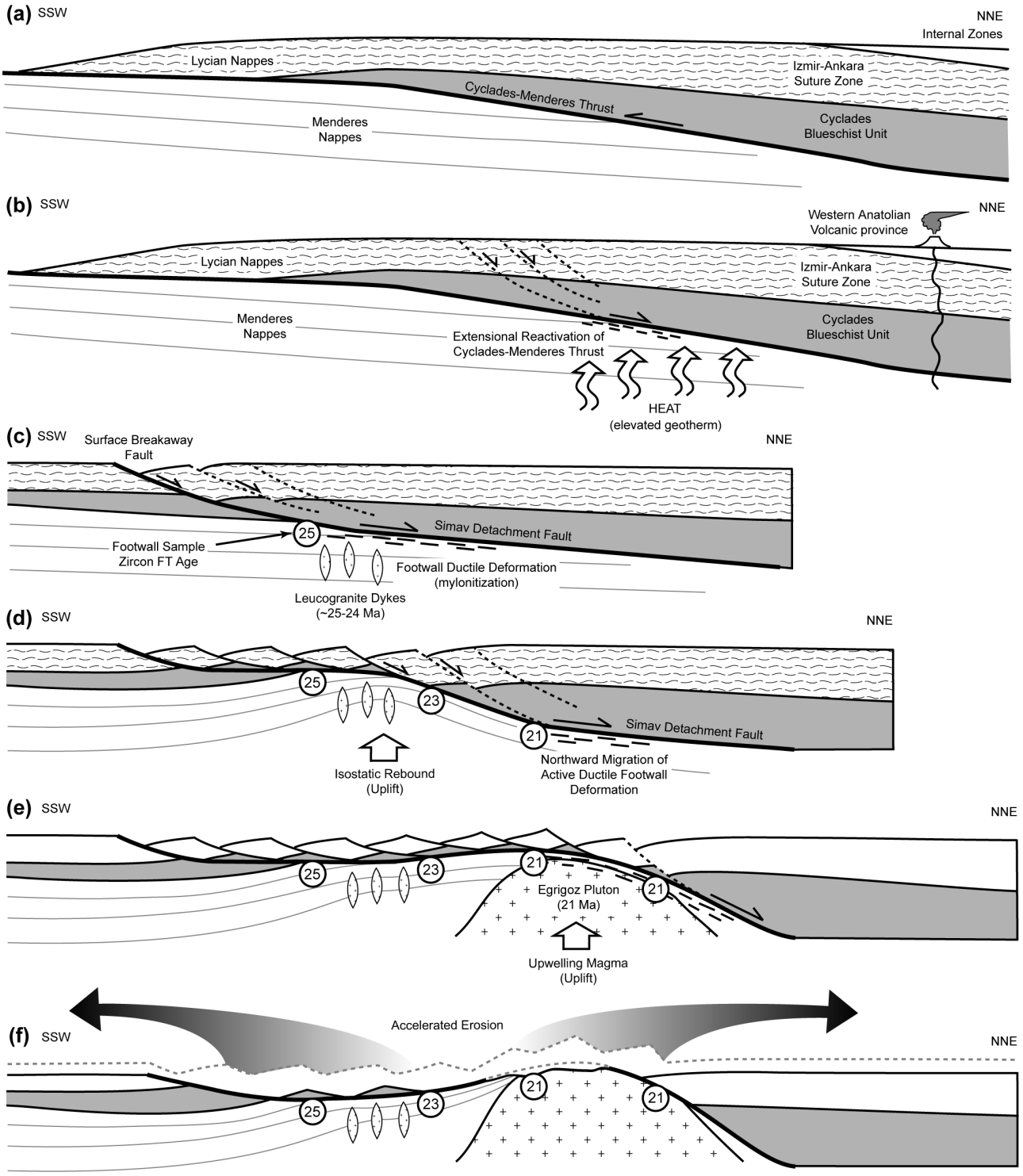

Figure 6. Cartoons illustrating the temporal evolution of the Cyclades Menderes thrust and the Simav detachment fault (SDF). (a) Early Oligocene situation after Anatolide orogen thrust belt had formed. (b and c) Late Oligocene extensional reactivation of Cyclades Menderes thrust by SDF and associated intrusion of leucogranite dikes. Note that development of SDF is largely controlled by brittle/ductile transition. (d) Northward migration of footwall deformation and initial isostatic rebound. (e) Early Miocene intrusion of Eğrigöz and Koyunoba granites in response to crustal extension. (f) Granite intrusions that ultimately led to uplift and doming of the SDF footwall, cessation of extension by ~19 Ma, and accelerated regional erosion.

normal reactivation of a major thrust in southern Nevada, while *Çemen and Wright* [1990] and *Miller* [2003] have described extensional overprinting of earlier basement thrust faults in the Death Valley region of California. Furthermore, *Parsons and Thompson* [1993] proposed that synextensional magmatism, and in particular dike intrusion, can provide the stress heterogeneity required to initiate low-angle normal faulting. Dating of white-mica fish records continued quartz-ductile extensional behavior of the northern SDF at 22.9 Ma [*Işik et al.*, 2004]. Older ZFT ages farther south indicate that at this time the footwall rocks here were already at temperatures below 280 ± 30°C (i.e., under brittle conditions), and hence that ductile deformation of the SDF migrated slowly northward with time. Renewed widespread synkinematic footwall magmatism in the form of the ~21–20 Ma Eğrigöz and Koyunoba plutons [*Ring and Collins*, 2005], perhaps at this time in response to crustal extension, appears ultimately to have led to uplift and doming of the SDF footwall and the cessation of extension by ~19 Ma (Figures 6e and 6f). *Ring and Collins* [2005] similarly speculated that the intrusion of the granites changed the stress geometry and rheology in such a way that caused the detachment to eventually become locked. The total amount of extensional offset represented by the SDF is difficult to accurately determine from the thermochronologic data alone. The total time of activity between ~25 and ~19 Ma and the approximate time-averaged slip rate of ~15 km/Myr imply an apparently high offset somewhere around ~90 km. The possibility of syndetachment erosion and thermal relaxation means that this estimate should be treated as a maximum, although the lateral extent of the exposed footwall of the SDF undoubtedly demonstrate that it was a very large scale detachment system. Following cessation of movement on the SDF, isostatic adjustment would have caused continued uplift (doming) leading to regional erosion, predominantly of the more easily eroded hanging wall rocks of the SDF, until ~16 Ma, when the footwall rocks (and some hanging wall klippen) of the SDF were unconformably overlain by the sedimentary rocks of the Selendi and Gördes basins.

[39] The remarkable coincidence between the onset of postcollision extension and magmatism at the northern margin of the Anatolide orogen at around ~25–24 Ma has important implications regarding the crustal dynamic processes leading to the late Cenozoic transition from collision to extension of the Anatolide belt of western Turkey. For example, did crustal extension (as the result of gravitational spreading of previously thickened crust or subduction retreat) initiate crustal melting that further enhanced extension (perhaps resulting in a positive feedback effect)?, or did crustal melting (induced by lithospheric delamination and/or accelerated slab rollback [e.g., *Aldanmaz et al.*, 2000; *Thomson et al.*, 1999]) result in crustal weakening aiding the development of the Simav low-angle detachment fault? Our data and the geologic relationships between deformation and prekinematic and synkinematic magmatism [e.g., *Ring and Collins*, 2005] favors the latter, and implies that the deeper mantle processes responsible for the onset of magmatism (e.g., lithospheric delamination or asthenospheric inflow into the back-arc mantle wedge following accelerated slab rollback) may have played an important role in the transition of the convergent Anatolide orogen to a region dominated by postcollision extension with the development of detachment faults.

7. Conclusions

[40] This study demonstrates that data obtained from multiple low-temperature thermochronometers are an essential tool in constraining the timing, magnitude and style of extension, especially in convergent orogenic settings such as western Anatolia where many of the tectonic contacts have been later tilted and folded, where out-of-sequence thrusts have been identified that juxtapose high- and low-pressure rocks of varying age, where extensional reactivation of older thrust faults may have occurred, and where kinematic, stratigraphic, or metamorphic data are lacking or ambiguous. Furthermore, such data provide vital information to help determine which geodynamic model or combination of models best describes the driving forces behind the presence of crustal extension following collision within a convergent orogen. This is especially true when such data are integrated with independent evidence on the timing of associated magmatism, sedimentation, and convergent tectonics.

[41] We confirm that the SDF was a major low-angle extensional detachment fault active sometime between ~25 and ~19 Ma. Also, despite widespread intrusion of late synkinematic granitoids destroying much information on the footwall unroofing history typically gained from applying low-temperature thermochronology, such as quantifying slip rates, changes in slip rate, total extensional offset, paleogeothermal gradient, and the timing of onset of footwall unroofing, the thermochronologic data still provide a number of key new constraints on previously contentious issues such as the timing, magnitude and nature of early postcollision extensional faulting at the northern margin of the Menderes massif and the western Anatolide orogen of western Turkey. Other conclusions more specific to the SDF are as follows:

[42] 1. ZFT cooling ages from the basement of the Gördes submassif, less influenced by Miocene plutonism, record rapid footwall cooling between ~25 and ~19 Ma consistent with other radiometric data [*Ring et al.*, 2003a; *Işik et al.*, 2004] and imply that the intrusion of the synkinematic Eğrigöz and Koyunoba plutons occurred once the fault was already active. Furthermore, the ZFT ages indicate that footwall ductile deformation and mylonitization along the southern exposed segments of the SDF away from the influence of early Miocene plutonism must have ceased sometime before ~23.6 ± 2.2 Ma. The synemplacement ductile deformation of the Eğrigöz and Koyunoba granites at ~21–20 Ma farther north [*Ring and Collins*, 2005] suggests that the active ductile deforming part of the SDF migrated northward with time.

[43] 2. Assuming the cooling ages were related to the removal of the hanging wall by top-to-the-NNE detachment faulting, the variation in ZFT ages in hanging wall slip

direction of the Gördes submassif define a fast minimum slip rate of ~15 km/Myr. However, the possibility of syndetachment erosion and thermal relaxation means that this estimate should be treated as a maximum.

[44] 3. Concordant AHe ages from the hanging wall and footwall of the SDF demonstrate that relative extensional offset on the SDF had all but ceased by ~19 Ma.

[45] 4. The near concordance of the AHe, ZFT and some AFT ages with the crystallization age of the Miocene (~21 Ma) granitoids reflects very rapid postemplacement cooling to below ~110°C within a few million years. This supports the fast cooling rates determined by *Ring and Collins* [2005] implying that these plutons were intruded at a very shallow crustal level. The close coincidence in timing of granite emplacement with the cessation of SDF activity suggests that these plutons acted to rotate the detachment surface causing the detachment to lock-up.

[46] 5. AFT ages from the footwall of the SDF are spatially invariant over >100 km, and consistently ~2–3 Ma younger than the ZFT ages from the same samples. Such an age pattern is consistent with a regional, relatively rapid erosion-linked cooling phase that postdates cessation of SDF activity at ~19 Ma.

[47] 6. Furthermore, the invariant AFT data imply that the SDF in the area investigated was active at temperatures >110 ± 10°C, and that ~2–3 km of overburden was removed from the Gördes submassif (i.e., above the detachment surface) following cessation of activity, but before deposition of unconformably overlying postdetachment sedimentary rocks of the Selendi and Gördes basins sometime before 16.4 ± 0.1 Ma.

[48] 7. Young AHe ages of 10–8 Ma close to the high-angle Pliocene-Recent Simav Graben fault reflect either renewed accelerated denudation at ~8 Ma, resetting by fault localized epithermal mineralization, or a paleo-HePRZ exhumed in the footwall of the younger fault in the last few million years. Note that the anomalously young (10 Ma) AFT age of sample THT25 close to Kula (Table 1 and Figure 2b) could reflect partial setting of this sample by the local Pleistocene-Recent Kula volcanic field.

[49] **Acknowledgments.** This work was funded by DFG grant Ri 538/15 to U.R. We thank Talip Güngör from İzmir University for continuous support of our work in western Turkey over the last 14 years. Fission track sample preparation was carried out at the Ruhr-Universität Bochum under the supervision of Frank Hansen. S.N.T. thanks Peter Reiners and Stefan Nicolescu for valuable support and technical assistance with (U-Th)/He sample analysis at Yale University. We also thank the Associate Editor Todd Ehlers and reviewers Ibrahim Çemen and Diane Seward, whose helpful comments and suggestions have resulted in a much improved and hopefully more readable manuscript.

References

Aldanmaz, E., J. A. Pearce, M. F. Thirwell, and J. G. Mitchell (2000), Petrogenetic evolution of late Cenozoic, post-collision volcanism in western Anatolia, Turkey, *J. Volcanol. Geotherm. Res.*, *102*, 67–95.

Axen, G. J. (1993), Ramp-flat detachment faulting and low-angle reactivation of the Tule Springs thrust, southern Nevada, *Geol. Soc. Am. Bull.*, *105*, 1076–1090.

Bozkurt, E. (2003), Origin of NE-trending basins in western Turkey, *Geodin. Acta*, *16*, 61–81.

Bozkurt, E., and R. Oberhänsli (2001), Menderes Massif (western Turkey): Structural, metamorphic and magmatic evolution—A synthesis, *Int. J. Earth Sci.*, *89*, 679–708.

Bozkurt, E., and R. G. Park (1994), Southern Menderes Massif: An incipient metamorphic core complex in western Anatolia, Turkey, *J. Geol. Soc. London*, *151*, 213–216.

Bozkurt, E., and M. Satir (2000), The southern Menderes Massif (western Turkey): Geochronology and exhumation history, *Geol. J.*, *35*, 285–296.

Brandon, M. T., M. K. Roden-Tice, and J. I. Garver (1998), Late Cenozoic exhumation of the Cascadia accretionary wedge in the Olympic Mountains, northwest Washington State, *Geol. Soc. Am. Bull.*, *110*, 985–1009.

Brichau, S., U. Ring, R. A. Ketcham, A. Carter, D. Stockli, and M. Brunel (2006), Constraining the long-term evolution of the slip rate for a major extensional fault system in the central Aegean, Greece, using thermochronology, *Earth Planet. Sci. Lett.*, *241*, 293–306.

Brix, M. R., B. Stöckhert, E. Seidel, T. Theye, S. N. Thomson, and M. Küster (2002), Thermobarometric data from a fossil partial annealing zone in high-pressure-low-temperature rocks of eastern and central Crete, Greece, *Tectonophysics*, *349*, 309–326.

Burchfiel, B. C., and L. Royden (1985), North-south extension within the convergent Himalayan region, *Geology*, *13*, 679–682.

Carlson, W. D., R. A. Donelick, and R. A. Ketcham (1999), Variability of apatite fission track annealing kinetics: I. Experimental results, *Am. Mineral.*, *84*, 1213–1223.

Carmignani, L., and R. Kligfield (1990), Crustal extension in the northern Apennines: The transition from compression to extension in the Alpi Apuane core complex, *Tectonics*, *9*, 1275–1303.

Carter, T. J., B. P. Kohn, D. A. Foster, and A. J. W. Gleadow (2004), How the Harcuvar Mountains metamorphic core complex became cool: Evidence from apatite (U-Th)/He thermochronometry, *Geology*, *32*, 985–988.

Catlos, E. J., and I. Çemen (2005), Monazite ages and rapid exhumation of the Menderes Massif, western Turkey, *Int. J. Earth Sci.*, *94*, 204–217.

Çemen, I., and L. A. Wright (1990), Effect of Cenozoic extension on Mesozoic thrust surfaces in the central and southern Funeral Mountains, Death Valley, California, in *Basin and Range Extensional Tectonics Near the Latitude of Las Vegas, Nevada*, edited by B. Wernicke, *Mem. Geol. Soc. Am.*, *176*, 305–316.

Chemenda, A. I., M. Mattauer, J. Malavieille, and A. N. Bokun (1995), A mechanism for syn-collisional rock exhumation and associated normal faulting: Results from physical modeling, *Earth Planet. Sci. Lett.*, *132*, 225–232.

Cohen, H. A., C. J. Dart, H. S. Akyüz, and A. Barka (1995), Syn-rift sedimentation and structural development of Gediz and Büyük Menderes grabens, western Turkey, *J. Geol. Soc. London*, *152*, 629–638.

Collins, A. S., and A. H. F. Robertson (1997), Lycian mélange, southwestern Turkey: An emplaced Late Cretaceous accretionary complex, *Geology*, *25*, 255–258.

Collins, A. S., and A. H. F. Robertson (1999), Evolution of the Lycian Allochthon, western Turkey, as north-facing Late Palaeozoic to Mesozoic rift and passive continental margin, *Geol. J.*, *34*, 107–138.

Davies, J. H., and F. von Blanckenburg (1995), Slab breakoff: A model of lithosphere detachment and its test in the magmatism and deformation of collisional orogens, *Earth Planet. Sci. Lett.*, *129*, 85–102.

Dewey, J. F. (1988), Extensional collapse of orogens, *Tectonics*, *7*, 1123–1139.

Ehlers, T. A., and K. A. Farley (2003), Apatite (U-Th)/He Thermochronometry: Methods and applications to problems in tectonics and surface processes, *Earth Planet Sci. Lett.*, *206*, 1–14, doi:10.1016/S0012-821X (02)01069-5.

England, P. C., and G. A. Houseman (1989), Extension during continental convergence, with application to the Tibetan Plateau, *J. Geophys. Res.*, *94*, 17,561–17,579.

Ercan, T., M. Satir, D. Sevin, and A. Turkecan (1997), Interpretation of radiometric age data on Tertiary-Quaternary volcanic rocks in W Anatolia, *Bull. Miner. Res. Explor. Inst. Turkey*, *119*, 103–112.

Farley, K. A. (2000), Helium diffusion from apatite I: General behavior as illustrated by Durango fluorapatite, *J. Geophys. Res.*, *105*, 2903–2914.

Farley, K. A. (2002), (U-Th)/He dating: Techniques, calibrations, and applications, in *Noble Gases in Geochemistry and Cosmochemistry*, edited by D. Porcelli, C. J. Ballentine, and R. Wieler, *Rev. Min. Geochem.*, vol. 47, pp. 819–844, Mineral. Soc. of Am., Washington, D. C.

Fassoulas, C., A. Kilias, and D. Mountrakis (1994), Postnappe stacking extension and exhumation of high pressure/low-temperature rocks in the island of Crete, Greece, *Tectonics*, *13*, 127–138.

Fossen, H. (1999), Extensional tectonics in the Caledonides: Synorogenic or postorogenic?, *Tectonics*, *19*, 213–224.

Foster, D. A., A. J. W. Gleadow, S. J. Reynolds, and P. G. Fitzgerald (1993), Denudation of metamorphic core complexes and the reconstruction of the transition zone, west central Arizona: Constraints from apatite fission track thermochronology, *J. Geophys. Res.*, *98*, 2167–2185.

Foster, D. A., and B. E. John (1999), Quantifying tectonic exhumation in an extensional orogen with

thermochronology: Examples from the southern Basin and Range province escape, in *Exhumation Processes: Normal Faulting, Ductile Flow and Erosion*, edited by U. Ring et al., *Geol. Soc. Spec. Publ.*, *154*, 87–107.

Galbraith, R. F., and G. M. Laslett (1993), Statistical models for mixed fission track ages, *Nucl. Tracks*, *21*, 459–470.

Gallagher, K. (1995), Evolving temperature histories from apatite fission-track data, *Earth Planet. Sci. Lett.*, *126*, 421–435.

Gallagher, K., R. W. Brown, and C. Johnson (1998), Fission track analysis and its application to geological problems, *Annu. Rev. Earth Planet. Sci.*, *26*, 19–72.

Gans, P. B., E. L. Miller, J. McCarthy, and M. L. Oldcott (1985), Tertiary extensional faulting and evolving ductile brittle transition zones in the northern Snake range and vicinity: New insights from seismic data, *Geology*, *13*, 189–193.

Gessner, K., U. Ring, C. Johnson, R. Hetzel, C. W. Passchier, and T. Güngör (2001a), An active bivergent rolling-hinge detachment system: The Central Menderes metamorphic core complex in western Turkey, *Geology*, *29*, 611–614.

Gessner, K., S. Piazolo, T. Güngör, U. Ring, A. Kröner, and C. W. Passchier (2001b), Tectonic significance of deformation patterns in granitoid rocks of the Menderes nappes, Anatolide belt, southwest Turkey, *Int. J. Earth Sci.*, *89*, 766–780.

Gessner, K., U. Ring, C. W. Passchier, and T. Güngör (2001c), How to resist subduction: Evidence for large-scale out-of-sequence thrusting during Eocene collision in western Turkey, *J. Geol. Soc. London*, *158*, 769–784.

Green, P. F., I. R. Duddy, G. M. Laslett, K. A. Hegarty, A. J. W. Gleadow, and J. F. Lovering (1989), Thermal annealing of fission tracks in apatite, 4, Quantitative modelling techniques and extension to geological timescales, *Chem. Geol.*, *79*, 155–182.

Hetzel, R., U. Ring, C. Akal, and M. Troesch (1995), Miocene NNE-directed extensional unroofing in the Menderes massif, western Turkey, *J. Geol. Soc. London*, *152*, 639–654.

House, M. A., K. A. Farley, and B. P. Kohn (1999), An empirical test of helium diffusion in apatite: Borehole data from the Otway Basin, Australia, *Earth Planet. Sci. Lett.*, *170*, 463–474.

Hurford, A. J. (1990), Standardization of fission track dating calibration: Recommended by the Fission Track Working Group of the I. U. G. S. Subcommission on Geochronology, *Chem. Geol.*, *80*, 171–178.

Hurford, A. J., and P. F. Green (1983), The zeta age calibration of fission-track dating, *Isot. Geosci.*, *1*, 285–317.

Hurford, A. J., J. C. Hunziker, and B. Stöckhert (1991), Constraints on the late thermotectonic evolution of the western Alps: Evidence for episodic rapid uplift, *Tectonics*, *10*, 758–769.

Ilkışık, O. M. (1995), Regional heat flow in western Anatolia using silica temperature estimates from thermal springs, *Tectonophysics*, *244*, 175–184.

Işik, V., and O. Tekeli (2001), Late orogenic crustal extension in northern Menderes Massif (western Turkey): Evidence for metamorphic core complex formation, *Int. J. Earth Sci.*, *89*, 757–765.

Işik, V., G. Seyitoğlu, and I. Çemen (2003), Ductile-brittle transition along the Alaşehir detachment fault and its structural relationship with the Simav detachment fault, Menderes Massif, western Turkey, *Tectonophysics*, *374*, 1–18.

Işik, V., O. Tekeli, and G. Seyitoğlu (2004), The $^{40}Ar/^{39}Ar$ age of extensional ductile deformation and granitoid intrusion in the northern Menderes core complex: Implications for the initiation of extensional tectonics in western Turkey, *J. Asian Earth Sci.*, *89*, 757–765.

Ketcham, R. A. (1996), Thermal models of core-complex evolution in Arizona and New Guinea: Implications for ancient cooling paths and present-day heat flow, *Tectonics*, *15*, 933–951.

Ketcham, R. A., R. A. Donelick, and W. D. Carlson (1999), Variability of apatite fission track annealing kinetics III: Extrapolation to geological time scales, *Am. Mineral.*, *84*, 1235–1255.

Koçyiğit, A., H. Yusufoğlu, and E. Bozkurt (1999), Evidence from the Gediz graben for episodic two-stage extension in western Turkey, *J. Geol. Soc. London*, *156*, 605–616.

Kounov, A., D. Seward, D. Bernoulli, J.-P. Burg, and Z. Ivanov (2004), Thermotectonic evolution of an extensional dome: The Cenozoic Osogovo-Lisets core complex (Kraishte zone, western Bulgaria), *Int. J. Earth Sci.*, *93*, 1008–1024.

Kumerics, C., U. Ring, S. Brichau, J. Glodny, and P. Monié (2005), The extensional Messaria shear zone and associated brittle detachment faults, Aegean Sea, Greece, *J. Geol. Soc.*, *162*, 701–721, doi:10.1144/0016-764904-041.

Laslett, G. M., P. F. Green, I. R. Duddy, and A. J. W. Gleadow (1987), Thermal annealing of fission tracks in apatite, 2, A quantitative analysis, *Chem. Geol.*, *65*, 1–13.

Lister, G. S., and S. L. Baldwin (1996), Modelling the effect of arbitrary P-T-t histories on argon diffusion in minerals using the MacArgon program for the Apple Macintosh, *Tectonophysics*, *253*, 83–109.

Lister, G. S., G. Banga, and A. Feenstra (1984), Metamorphic core complexes of Cordilleran type in the Cyclades, Aegean Sea, Greece, *Geology*, *12*, 221–225.

Liu, M. (2001), Cenozoic extension and magmatism in the North American Cordillera: The role of gravitational collapse, *Tectonophysics*, *342*, 407–433.

Malavieille, J. (1993), Late orogenic extension in mountain belts: Insights from the Basin and Range and the late Paleozoic Variscan belt, *Tectonics*, *12*, 1115–1130.

Mantovani, E., M. Viti, D. Babbucci, C. Tamburelli, and D. Albarello (2001), Back arc extension: Which driving mechanism?, *J. Virtual Explorer*, *3*, 17–45.

Miller, E. L., T. A. Dumitru, R. W. Brown, and P. B. Gans (1999), Rapid Miocene slip on the Snake Range-Deep Creek Range fault system, east-central Nevada, *Geol. Soc. Am. Bull.*, *111*, 886–905.

Miller, M. (2003), Basement involved thrust faulting in a thin-skinned fold and thrust belt, Death Valley, California, USA, *Geology*, *31*, 31–34.

Okay, A. L. (2001), Stratigraphic and metamorphic inversions in the central Menderes Massif: A new structural model, *Int. J. Earth Sci.*, *89*, 709–727.

Okay, A. L., and M. Siyako (1993), The new position of the İzmir-Ankara Neo-Tethyan suture between İzmir and Balikesir, in *Tectonics and Hydrocarbon Potential of Anatolia and Surrounding Regions, Proceedings of the Ozan Sungurl Symposium, Ankara*, edited by S. Turgut, pp. 333–335, Turkish Assoc. of Pet. Geol., Ankara.

Özgür, N. (2002), Geochemical signature of the Kizildere Geothermal Filed, western Anatolia, Turkey, *Int. Geol. Rev.*, *44*, 153–163.

Parsons, T., and G. A. Thompson (1993), Does magmatism influence low-angle normal faulting?, *Geology*, *21*, 247–250.

Platt, J. P. (1986), Dynamics of orogenic wedges and the uplift of high-pressure metamorphic rocks, *Geol. Soc. Am. Bull.*, *97*, 1037–1053.

Platt, J. P., and R. L. M. Vissers (1989), Extensional collapse of thickened continental lithosphere: A working hypothesis for the Alboran Sea and the Gibraltar arc, *Geology*, *17*, 540–543.

Platt, J. P., M. J. Whitehouse, S. P. Kelley, A. Carter, and L. Hollick (2003), Simultaneous extensional exhumation across the Alboran Basin: Implications for the causes of late orogenic extension, *Geology*, *31*, 251–254.

Purvis, M., and A. H. F. Robertson (2004a), A pulsed extension model for the Neogene-Recent E-W-trending Alaşehir Graben and the NE-SW-trending Selendi and Gördes basins, western Turkey, *Tectonophysics*, *391*, 171–201.

Purvis, M., and A. H. F. Robertson (2004b), Sedimentation of the Neogene-Recent Alaşehir (Gediz) continental graben system used to test alternative tectonic models for western (Aegean) Turkey, *Sediment. Geol.*, *173*, 373–408.

Rahn, M. K., M. T. Brandon, G. E. Batt, and J. I. Garver (2004), A zero-damage model for fission-track annealing in zircon, *Am. Mineral.*, *89*, 473–484.

Régnier, J. L., U. Ring, C. W. Passchier, K. Gessner, and T. Güngör (2003), Contrasting metamorphic evolution of metasedimentary rocks from the Çine and Selimiye nappes in the Anatolide belt, western Turkey, *J. Metamorph. Geol.*, *21*, 699–721.

Rehrig, W. A., and S. J. Reynolds (1980), Geologic and geochronologic reconnaissance of a northwest-trending zone of metamorphic core complexes in southern and western Arizona, in *Cordilleran Metamorphic Core Complexes*, edited by M. D. Crittenden, P. J. Coney, and G. H. Davis, *Geol. Soc. Am. Mem.*, *153*, 131–156.

Reiners, P. W., Z. Zhou, T. A. Ehlers, C. Xu, M. T. Brandon, R. A. Donelick, and S. Nicolescu (2003), Post-orogenic evolution of the Dabie Shan, eastern China, from (U-Th)/He and fission-track dating, *Am. J. Sci.*, *303*, 489–518.

Rey, P., O. Vanderhaeghe, and C. Teyssier (2001), Gravitational collapse of the continental crust: Definition, regimes and modes, *Tectonophysics*, *342*, 435–449.

Reynolds, S. J., and J. E. Spencer (1985), Evidence for large-scale transport on the Bullard detachment fault, west-central Arizona, *Geology*, *13*, 353–356.

Ring, U., and A. S. Collins (2005), U-Pb SIMS dating of syn-kinematic granites: Timing of core-complex formation in the northern Anatolide belt of western Turkey, *J. Geol. Soc.*, *162*, 289–298.

Ring, U., and P. W. Layer (2003), High-pressure metamorphism in the Aegean, eastern Mediterranean: Sequential accretion from the Late Cretaceous until the Miocene to Recent, *Tectonics*, *22*(3), 1022, doi:10.1029/2001TC001350.

Ring, U., K. Gessner, T. Güngör, and C. W. Passchier (1999), The Menderes Massif of western Turkey and the Cycladic Massif in the Aegean—Do they really correlate?, *J. Geol. Soc. London*, *156*, 3–6.

Ring, U., A. P. Willner, and W. Lackmann (2001a), Stacking of nappes with different pressure-temperature paths: An example from the Menderes nappes of western Turkey, *Am. J. Sci.*, *301*, 912–944.

Ring, U., P. W. Layer, and T. Reischmann (2001b), Miocene high-pressure metamorphism in the Cyclades and Crete, Aegean Sea, Greece: Evidence for large-magnitude displacement on the Cretan detachment, *Geology*, *29*, 395–398.

Ring, U., C. Johnson, R. Hetzel, and K. Gessner (2003a), Tectonic denudation of a Late Cretaceous-Tertiary collisional belt: Regionally symmetric cooling patterns and their relation to extensional faults in the Anatolide belt of western Turkey, *Geol. Mag.*, *140*, 421–441.

Ring, U., S. N. Thomson, and M. Bröcker (2003b), Fast extension but little exhumation: The Vari detachment in the Cyclades, Greece, *Geol. Mag.*, *140*, 245–252.

Şengör, A. M. C. (1987), Cross faults and differential stretching in their hanging walls in regions of low-angle normal faulting: Examples from western Turkey, in *Continental Extensional Tectonics*, edited by M. J. Coward, J. F. Dewey, and P. L. Hancock, *Geol. Soc. London Spec. Publ.*, 28, 405–473.

Şengör, A. M. C., and Y. Yilmaz (1981), Tethyan evolution of Turkey: A plate tectonic approach, *Tectonophysics*, *75*, 181–241.

Seyitoğlu, G., and B. C. Scott (1992), Late Cenozoic volcanic evolution of the northeastern Aegean region, *J. Volcanol. Geotherm. Res.*, *54*, 157–176.

Seyitoğlu, G., and B. C. Scott (1996), The cause of N-S extensional tectonics in western Turkey: Tectonic escape vs back-arc spreading vs orogenic collapse, *J. Geodyn.*, *22*, 145–153.

Seyitoğlu, G., B. C. Scott, and C. C. Rundle (1992), Timing of Cenozoic extensional tectonics in west Turkey, *J. Geol. Soc. London*, *149*, 533–538.

Seyitoğlu, G., I. Çemen, and O. Tekeli (2000), Extensional folding in the Alaşehir Graben, West Anatolia, Turkey, *J. Geol. Soc. London*, *157*, 1097–1100.

Seyitoğlu, G., O. Tekeli, I. Çemen, S. Sen, and V. Işik (2002), The role of the flexural rotation/rolling hinge model in the tectonic evolution of the Alasehir graben, western Turkey, *Geol. Mag.*, *139*, 15–26.

Seyitoğlu, G., V. Işik, and I. Çemen (2004), Complete Tertiary exhumation history of the Menderes massif, western Turkey: An alternative working hypothesis, *Terra Nova*, *16*, 358–364.

Sherlock, S., S. P. Kelley, S. Inger, N. Harris, and A. I. Okay (1999), ^{40}Ar-^{39}Ar and Rb-Sr geochronology of high-pressure metamorphism and exhumation history of the Tavsanli Zone, NW Turkey, *Contrib. Mineral. Petrol.*, *137*, 46–58.

Sonder, L. J., and C. H. Jones (1999), Western United States extension: How the west was widened, *Annu. Rev. Earth Planet. Sci.*, *27*, 417–462.

Stöckhert, B., M. R. Brix, R. Kleinschrodt, A. J. Hurford, and R. Wirth (1999), Thermochronology and microstructures of quartz—A comparison with experimental flow laws and predictions on the temperature of the brittle-plastic transition, *J. Struct. Geol.*, *21*, 351–369.

Tagami, T., R. F. Galbraith, R. Yamada, and G. M. Laslett (1998), Revised annealing kinetics of fission tracks in zircon and geological implications, in *Advances in Fission-Track Geochronology*, edited by P. Van den haute and F. De Corte, pp. 99–112, Springer, New York.

Thomson, S. N. (1998), Assessing the nature of tectonic contacts using fission-track thermochronology: An example from the Calabrian Arc, southern Italy, *Terra Nova*, *10*, 32–36.

Thomson, S. N., B.Stöckhert, and M. R. Brix (1999), Miocene high-pressure metamorphic rocks of Crete, Greece: Rapid exhumation by buoyant escape, in *Exhumation Processes: Normal Faulting, Ductile Flow and Erosion*, edited by U. Ring et al., *Geol. Soc. Spec. Publ.*, *154*, 87–108.

Tomaschek, F., A. K. Kennedy, I. M. Villa, M. Lagos, and C. Ballhaus (2003), Zircons from Syros, Cyclades, Greece—Recrystallization and mobilization of zircon during high-pressure metamorphism, *J. Petrol.*, *44*, 1977–2002.

Wheeler, J., and R. W. H. Butler (1994), Criteria for identifying structures related to true crustal extension in orogens, *J. Struct. Geol.*, *16*, 1023–1027.

Wolf, R. A., K. A. Farley, and D. M. Kass (1998), Modeling of the temperature sensitivity of the apatite (U-Th)/He thermochronometer, *Chem. Geol.*, *148*, 105–114.

Yilmaz, Y., S. C. Genç, O. F. Gürer, M. Bozcu, K. Yilmaz, Z. Karacik, S. Altunkaynak, and A. Elmas (2000), When did the western Anatolian grabens begin to develop?, in *Tectonics and Magmatism in Turkey and the Surrounding Area*, edited by E. Bozkurt, J. A. Winchester, and J. A. D. Piper, *Geol. Soc. Spec. Publ.*, *173*, 353–384.

Zeilinga de Boer, J. (1989), The Greek enigma: Is development of the Aegean Orogen dominated by forces related to subduction or obduction?, *Mar. Geol.*, *87*, 31–54.

U. Ring, Department of Geological Sciences, University of Canterbury, Private Bag 4800, Christchurch 8020, New Zealand. (uwe.ring@canterbury.ac.nz)

S. N. Thomson, Department of Geology and Geophysics, Yale University, P.O. Box 208109, New Haven, CT 06520-8109, USA. (stuart.thomson@yale.edu)